Electronic Supplementary Information for

Developing the mechanism of dioxygen reduction catalyzed by multicopper oxidases using protein film electrochemistry

James A. Cracknell and Christopher F. Blanford

Table of contents

Section S1 Measuring the rate of O_2 saturation

We measured the time required for 2 mL buffer solution in the electrochemical cell to become saturated with O_2. A freshly-sanded graphite electrode was placed in the electrochemical cell containing (air-saturated) buffer and was rotated at 4000 rpm. The electrode was poised at a negative potential at which O_2 is reduced at the graphite surface. This potential is lower than probed in any of the experiments described in the manuscript. At 0 s the cell was flushed with O_2, and the O_2 reduction current monitored. As can be seen in Figure S1, the cell solution is saturated with O_2 after approximately 300 s, as measured by the stable current response after this time. In order to ensure that our observations were not due to the effects of saturating the cell solution with O_2, the cell was typically flushed with O_2 for at least 600 s prior to the starting any experiment.

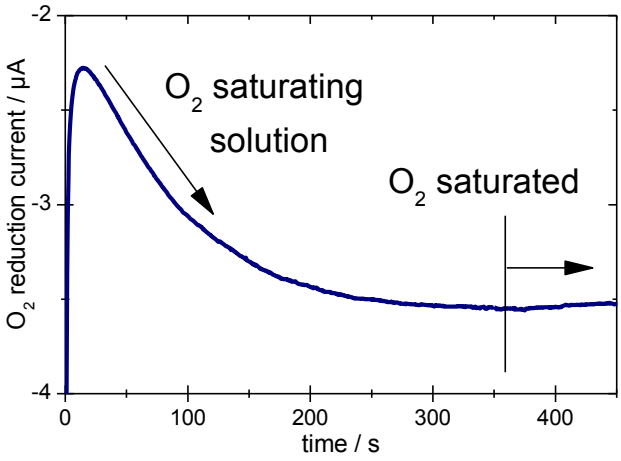

Figure S1. O_2 reduction current at a bare graphite electrode. The cell solution was initially in equilibrium with air (i.e., not saturated with O_2); O_2 was flushed through the cell starting at time = 0 s. $E_{applied}$ = –0.15 V *vs.* SHE; pH 4.0 (0.1 M phosphate); ω = 4000 rpm; T = 25 °C; solution volume = 2 ml.

Section S2 Observation of the X State in other multicopper oxidases

We performed measurements analogous to those described in the main text for *Tv* L (Figure 4A) to determine whether BMCOs from other organisms also form the X state during catalysis at high pH. Our results (Figure S2) show that X State formation is common to both high potential BMCOs (*Mv* BOx in addition to *Tv* L) and low-potential enzymes (*Bs* CotA and *Rv* L).

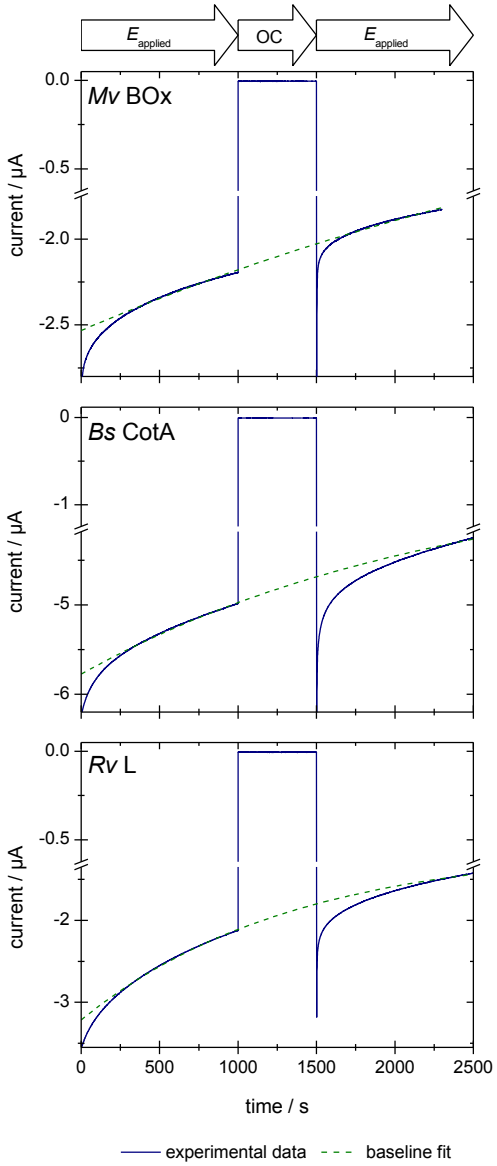

Figure S2. Evidence of X State formation in three multicopper oxidases: bilirubin oxidase from the ascomycete fungus *Myrothecium verrucaria* (*Mv* BOx), spore coat protein CotA from the bacterium *Bacillus subtilis* (*Bs* CotA), and plant laccase from *Rhus vernicifera* (*Rv* L). X State formation is seen as an increase in catalytic current (relative to the baseline) following a period at open circuit. All data were obtained at pH 7.5, 0.1 M phosphate, T = 25 °C, ω = 4000 rpm, $E_{applied}$ = 0 V vs. SCE, with the electrolyte solution saturated with O_2 prior to the start of the experiment. "OC" stands for open circuit, when no potential is applied to the working electrode.

Section S3 Cyclic voltammetry of *Tv* L over a wider potential range

Cyclic voltammograms of *Tv* L were recorded under conditions identical to those shown in Fig. 1 but extending to a potential 0.2 V lower (Figure S3). No additional features appeared at the lower potential. Each scan was 140 s instead of 100 s, so the re-activation was complete after the first potential cycle.

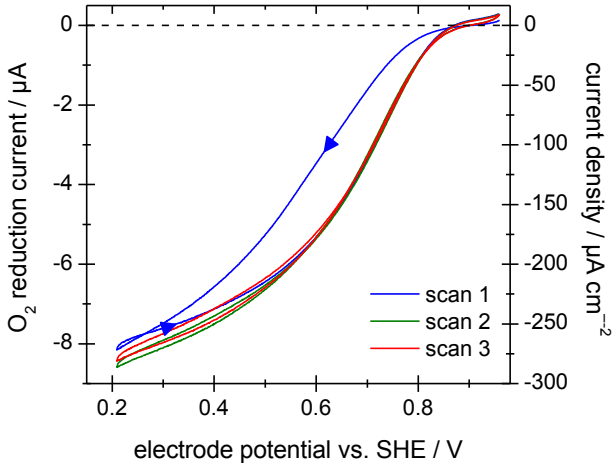

Figure S3. Cyclic voltammograms of laccase from *Trametes versicolor* on a pyrolytic graphite electrode modified with aminoanthracene, showing an activation process in the first potential cycle that disappears in subsequent sweeps. Experimental conditions were: υ = 10 mV s^{-1}, 0.1 M phosphate pH 4.0, T = 25 °C, ω = 4000 rpm, A = 3 mm^2, 1 atm O_2 (solution pre-saturated prior to experiment).

Section S4 Reaction schemes that were modeled

Our simulations (described in the main text) allowed the unambiguous positioning of the X State in the catalytic cycle. The three schemes that were modeled (see Analysis, main text) are shown below (Figure S4 – Figure S6).

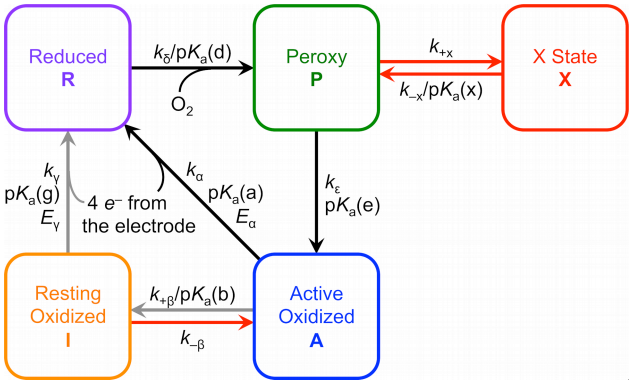

Figure S4. "P deadend scheme". The X State is formed from the Peroxy Intermediate and reverts to the same and the rate of consumption of the X State depends on proton concentration. The bold letters in each box are the one-letter codes we used in our mathematical models and simulations. This scheme is identical to Scheme 1 in the main text of the manuscript.

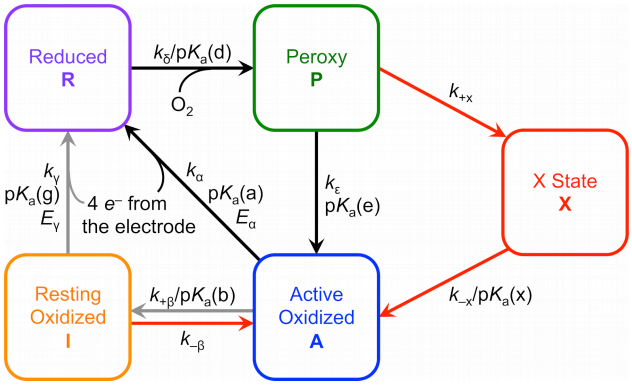

Figure S5. "P bridge scheme". The X State is formed from the Peroxy Intermediate which then forms the Active Oxidized form and the rate of consumption of the X State depends on proton concentration.

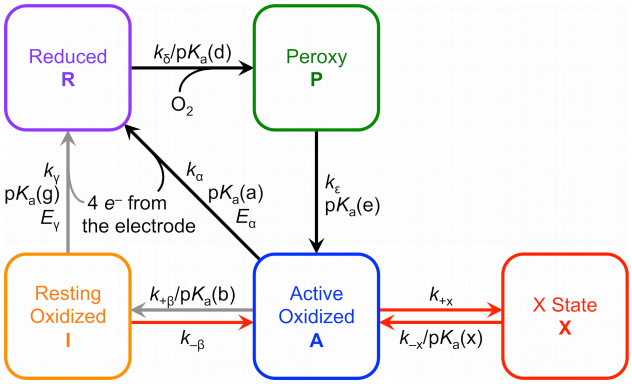

Figure S6. "A deadend scheme". The X State is formed from the Active Oxidized form and reverts to the same and the rate of consumption of the X State depends on proton concentration.

Section S5 Effect of internal weak acids and bases on apparent reaction order with respect to [H^+]

When the rate-limiting step in an enzymatic reaction depends on [H^+], a plot of rate versus pH gives a sigmoidal shape (cf. Eqn. S1 and Figure S7A). The midpoint of that shape is commonly related to the pK_a of an ionizable amino acid side chain, such as the carboxylates on aspartate or glutamate residues. In contrast to conventional reaction kinetics, in which the rate order with respect to a reactant is constant, the apparent rate order (Eqn. S2) varies with pH (Eqn. S3).

$$k^{\text{obs}} = (k^{\text{low pH}} - k^{\text{high pH}}) \left(1 - \frac{1}{1 + 10^{\text{p}Ka - \text{pH}}}\right) + k^{\text{high pH}} \tag{S1}$$

$$z = -\frac{\text{d} \log_{10}(k^{\text{obs}})}{\text{d(pH)}} \tag{S2}$$

$$z = \frac{(k^{\text{low pH}} - k^{\text{high pH}})\ 10^{\text{pH}+\text{p}Ka}}{(10^{\text{pH}} + 10^{\text{p}Ka})\ (k^{\text{high pH}}\ 10^{\text{pH}} + k^{\text{low pH}}\ 10^{\text{p}Ka})} \tag{S3}$$

where k^{obs} is the pH-dependent rates; $k^{\text{low pH}}$ and $k^{\text{high pH}}$ are the limiting rates at low and high pH values, respectively; and z is the apparent rate order with respect to [H^+]. In the simplest case, where $k^{\text{high pH}} = 0$ (or $k^{\text{low pH}} \gg k^{\text{high pH}}$) then the rate order reduces to Eqn. S4, the apparent rate order = ½ when pH = pK_a, and approaches 1 at pH values much greater than the pK_a (red line, Figure S7B).

$$z = -\frac{1}{1 + 10^{\text{p}Ka - \text{pH}}} \tag{S4}$$

In the more complex case, where $k^{\text{high pH}}$ is not negligible, the apparent order reaches a maximum (z^{max}) less than 1 at $\text{pH}^{z\ \text{max}}$:

$$z^{\text{max}} = \frac{k^{\text{low pH}} - k^{\text{high pH}}}{\left(1 + \sqrt{\frac{k^{\text{high pH}}}{k^{\text{low pH}}}}\right)\left(k^{\text{low pH}} \sqrt{\frac{k^{\text{high pH}}}{k^{\text{low pH}}}} + k^{\text{high pH}}\right)} \tag{S5}$$

$$\text{pH}^{z\ \text{max}} = \text{p}K_a - \frac{1}{2} \log_{10} \frac{k^{\text{high pH}}}{k^{\text{low pH}}} \tag{S6}$$

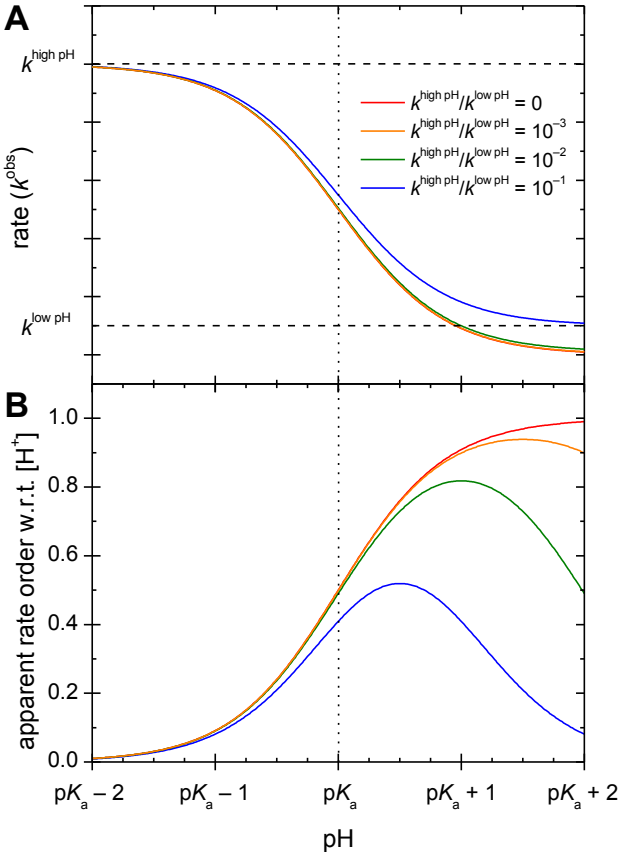

Figure S7. The dependence of pH on reaction rates and its dependence on apparent reaction order with respect to proton concentration. Panel A shows the simulated sigmoidal pH dependence on reaction rate. Panel B shows how the apparent reaction order varies with pH, pK_a, and ratio of rates at low and high pH values.

Section S6 Variation in pH activity profiles between solution- and PFE-based assays

Variable potential differences between the MCO and the soluble reducing agent. The shift in reduction potential of the reducing agent should be relatively uniform with pH, regardless of whether it is a "zero-proton, one-electron donor" like ABTS or a "one-proton, one-electron" donor such as catechol. Our simulations of E_{cat} vs. pH (Fig. 5), which account for both thermodynamic and kinetic effects on activity, predict changes in potential that vary widely from the –60 mV (–ln(10) RT/F) shift per pH unit predicted by the thermodynamics of the O_2-reduction reaction, with little or no change in E_{cat} at the extreme potentials. The effect on the pH–activity curves will be larger when either a "one-proton, one-electron donor" is used with an enzyme with low k_α^{max}, where $dE_{cat}/d(pH)$ will be relatively constant but the reduction potential of the donor will shift by ca. –60 mV per pH unit; or the converse case with a "zero-proton, one-electron" with a high k_α^{max}. The effect will always be greater when the potential of the electron donor is close to E_{cat} of the enzyme.

Increasing fraction of Resting Oxidized state at low pH. In solution assays, the activity drop reported at low pH values may due to a higher fraction of Resting Oxidized state (Figs. 4B and 8) and its slow reactivation. For *Tv* L, for example, we predict that up to two-thirds of the enzyme is in the Resting Oxidized state at pH 3, about twice the fraction as at pH 5. Unless the enzyme is pre-reduced in the absence of O_2 (as is done for many stopped-flow measurements) the enzyme is unlikely to be fully active in the assay: about 50 s is required to reach 95% of its steady-state activity on an electrode; it will take longer in solution because of substrate and product diffusion. However, even in PFE assays in which diffusion is eliminated or mathematically factored out, we and others have observed a decrease in catalytic activity that is at least partly reversible (Lee et al., *J. Electroanal. Chem. Interfacial Electrochem.,* 1984, **172,** 289–300; Thuesen et al., *Acta Chem. Scand.,* 1998, **52,** 555–562). Our model does not predict this behavior, which suggests that there is another, less active state or conformation of the enzyme that dominates at low pH values.

Reduction in catalytic activity at high pH. For solution assays of MCOs from many species, this decrease has been attributed to hydroxide inhibition (Xu, *Appl. Biochem. Biotechnol.,* 2001, **95,** 125–

133; Xu, *J. Biol. Chem.,* 1997, **272,** 924–928). However, it now seems more likely that the loss is simply due to decreasing fractions of protonation of essential acid amino acid residues. At pH values above the inflection point in a E_{cat} vs. pH trace (e.g., Fig. 5), the formal potential of the $O_2/2H_2O$ couple rapidly approaches the value for E_{cat}, consistent with previous observations (dos Santos et al., *Phys. Chem. Chem. Phys.*, 2010, **12,** 13962-13974). At the same time, however, the potential of this couple approaches the reversible potential of the putative primary electron acceptor, the T1 Cu (Fee et al., *Biochim. Biophys. Acta*, 1970, **197,** 136–142.) which has a potential that changes comparably little with pH (Xu, 1997, ibid.). This translates into a decreased driving force for O_2 reduction at higher pH values. This may be the origin of the higher pH optima in MCOs which have a lower T1 Cu potential than *Tv* L (e.g., *Rv* L, *Mv* BOx, *Ec* CueO); higher pH values are required for the formal reduction potential of O_2 to approach that of the T1 Cu allowing kinetic activity to persist (Kamitaka et al., *J. Electroanal. Chem.*, 2007, **601,** 119–124).

Section S7 Selected model sensitivity analyses

Each of the experimentally measured quantities shown in Figs. 2B, 4B and 5–8 in the main text is influenced by several of the model variables. To illustrate this, the effect of changes in individual variables is shown in the simulations in Figure S8 – Figure S16.

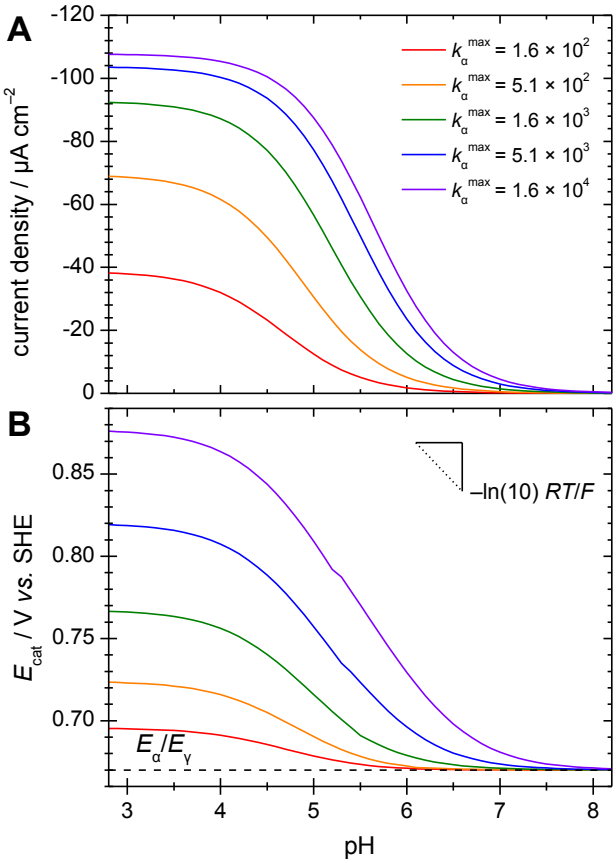

Figure S8. The effect of k_α on the pH dependence of current density and E_{cat} (cf. Fig. 5). In each case all the other constants are the same as in Table 1 in the main text. The center green line represents the constant used in the simulations in the main text.

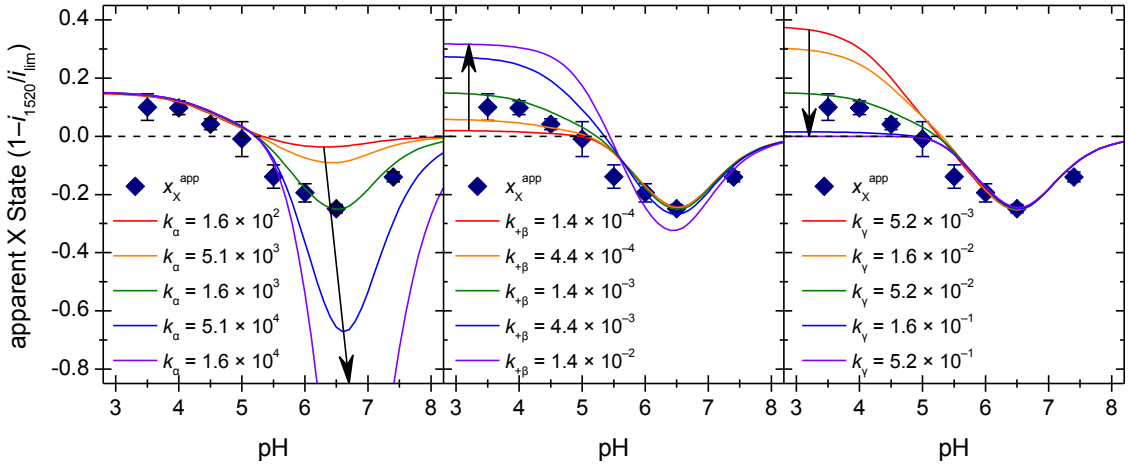

Figure S9. The effect of k_α, k_β and k_γ on the apparent fraction of enzyme in the X State (x_X^{app}) (cf. Fig. 4B). In each case all the other constants are the same as in Table 1 in the main text. The center green line represents the constant used in the simulations in the main text.

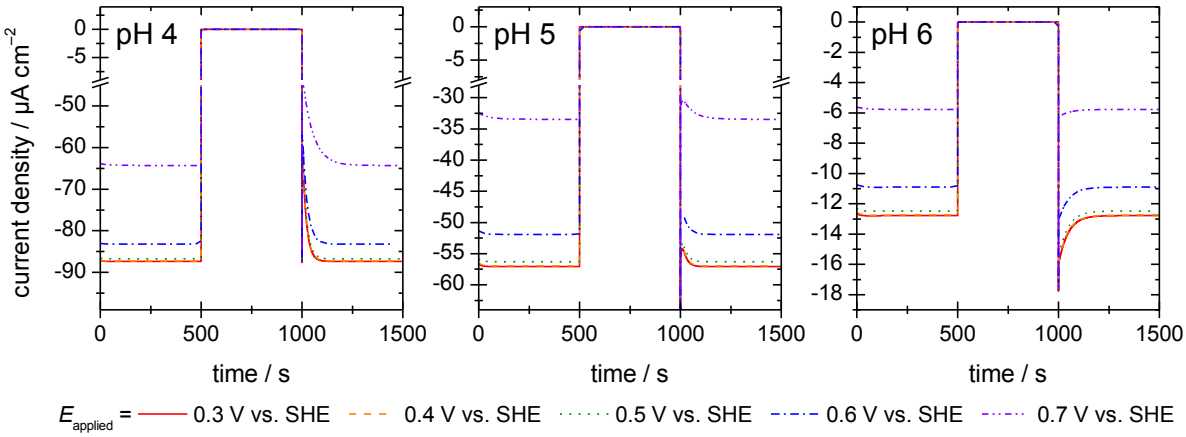

Figure S10. The effect of varying the applied potential ($E_{applied}$) on simulations of chronoamperometric traces at different pH values (cf. Fig. 8, middle panels). The potential is applied from 0 to 500 s and from 1000 to 1500 s; from 500 to 1000 s, the system is at open circuit. Applied potentials must be at least 0.2 V above what was used in the simulations (0.4 V vs. SHE at pH 4), even without adjusting $E_{applied}$ for pH, before any significant change (>5% from the maximum value) is observed.

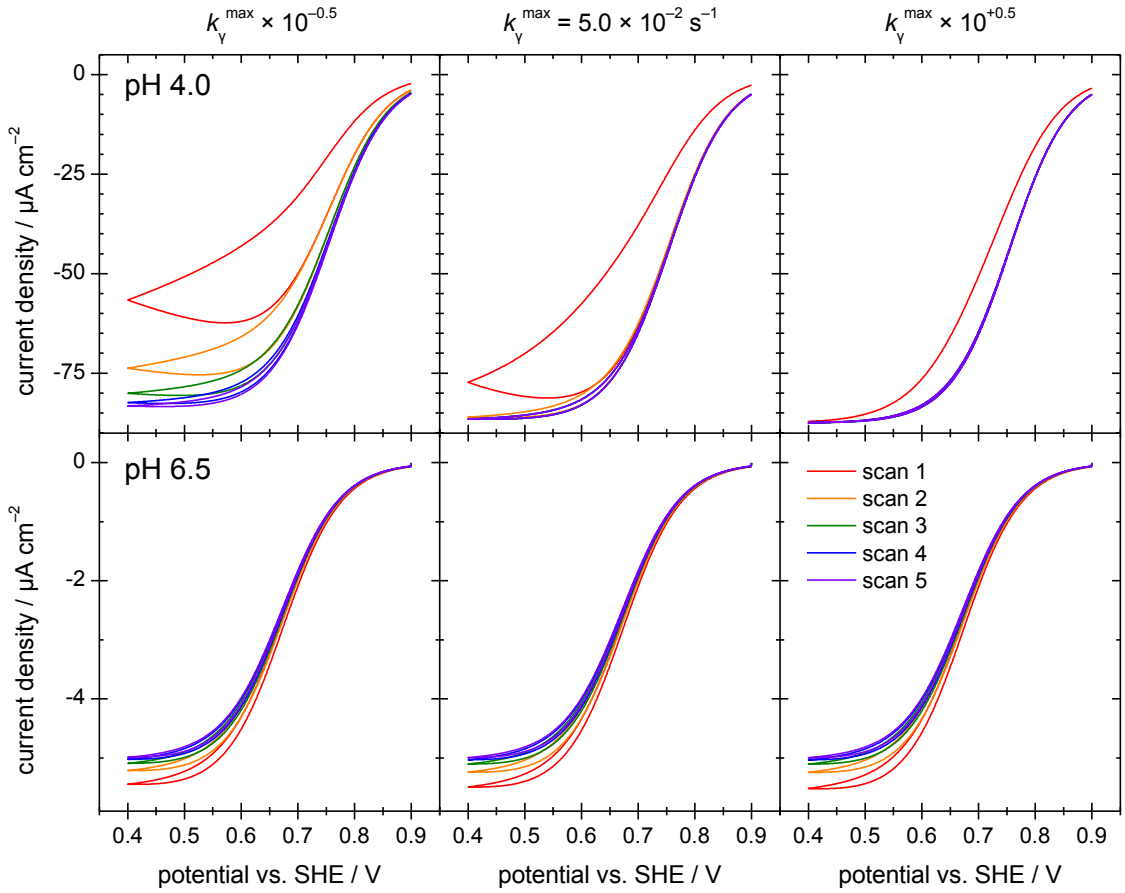

Figure S11. The effect of k_γ on activation rate in CVs (cf. Fig. 7). The reactivation from the Resting Oxidized state is prominent only at lower pH values. The simulated scan rate is 10 mV s^{-1}, with the initial sweep being in the reductive direction (i.e., 0.9 → 0.4 → 0.9 V vs. SHE). Other conditions are as in the main text and Table 1.

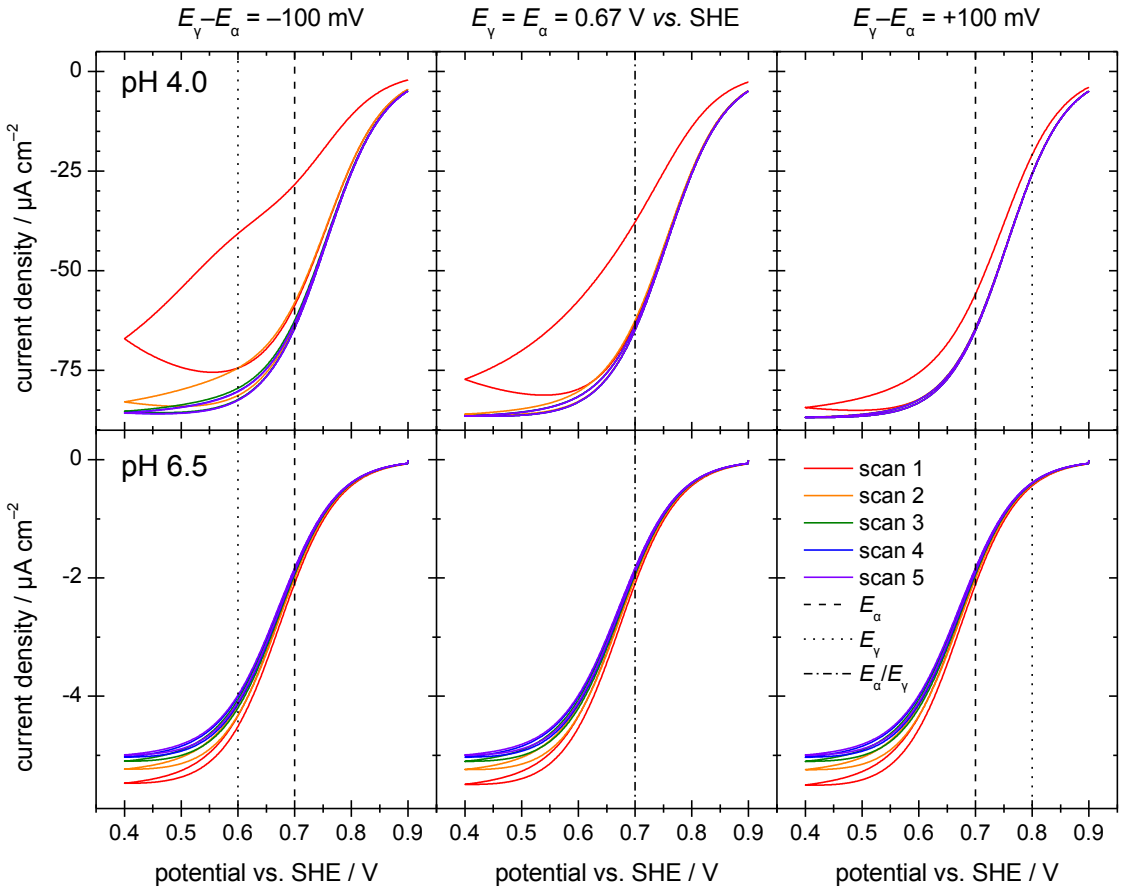

Figure S12. The effect of (E_γ–E_α) on shape of CVs (cf. Fig. 7). When is E_γ is lower than E_α (left panels), a second distinct bump appears in the first scan (although the position of E_{cat} — the maximum in d*i*/d*E* — remains the same) and the overall reactivation process is slower. The contrasting case in the right panels shows an effective increase in the rate of activation because the activation process occurs before and at a higher rate than the reduction step associated with the normal catalytic cycle. The effects of reactivation from the Resting Oxidized state only manifest themselves at lower pH values. The simulated scan rate is 10 mV s^{-1}, with the initial sweep being in the reductive direction (i.e., 0.9 → 0.4 → 0.9 V vs. SHE). Other conditions are as in the main text and Table 1.

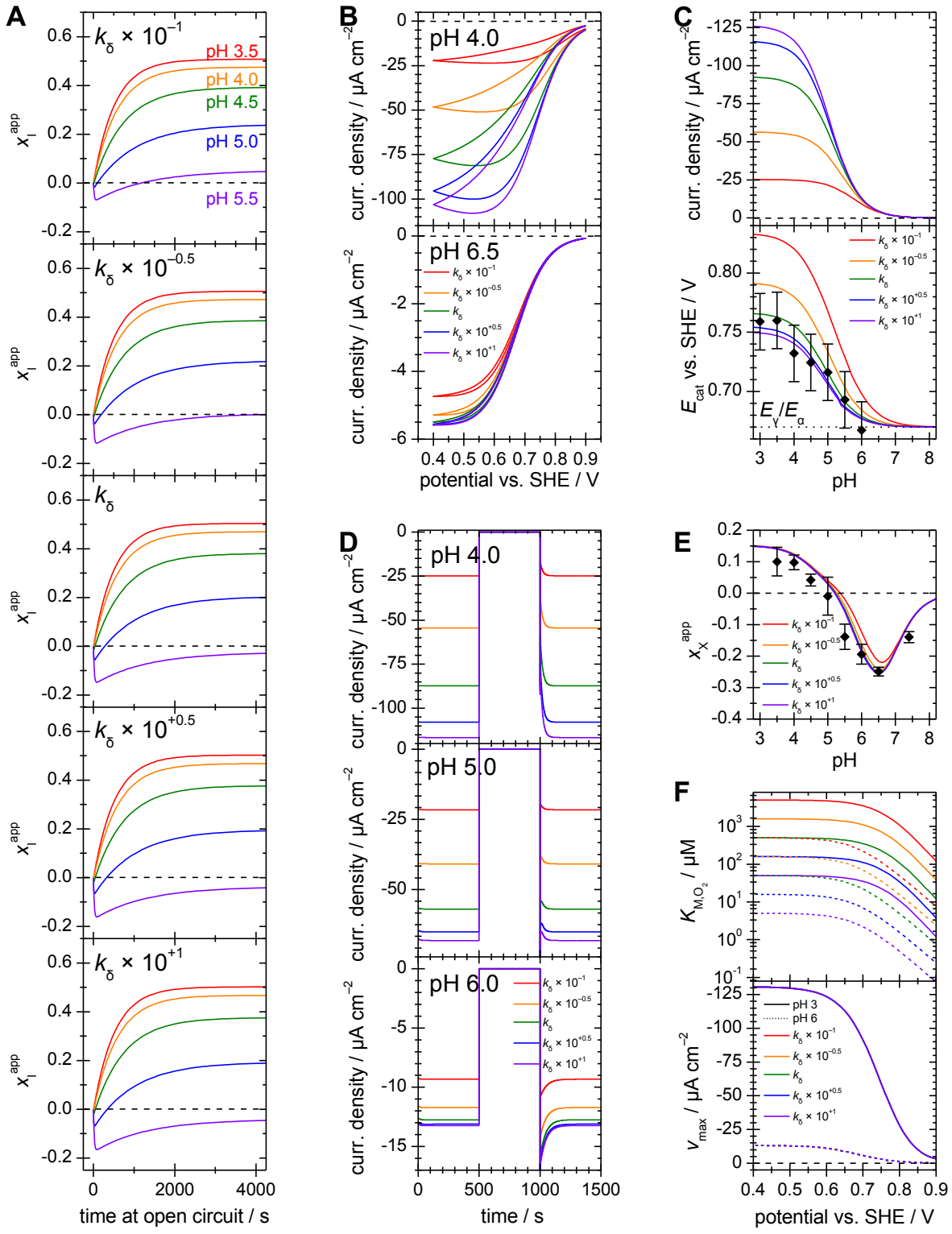

Figure S13. Graphical illustration of the effect of varying k_δ over two orders of magnitude, with the center value (green line in parts B–F) the same as that used in the figures in the main text. With increasing k_δ there is (A) almost no effect on the apparent fraction inactivated (x_I^{app}) with pH and time at open circuit except at pH 5.5 (cf. Fig. 2B); (B) a small increase in current at low pH, but no difference in activation rate at low or high pH (first scan, 10 mV s^{-1}, cf. Fig. 7); (C) an increase in catalytic activity and decrease in E_{cat} at low pH (cf. Fig. 5); (D) an increase in steady-state catalytic activity at low pH, but no change in activation profile (cf. Fig. 8, middle panels); (E) little change in apparent fraction of X State (x_X^{app}) (cf. Fig. 4B); and (F) a marked decrease in $K_{M,O2}$ at both low and high pH values, with no change in v_{max} (cf. Fig. 6).

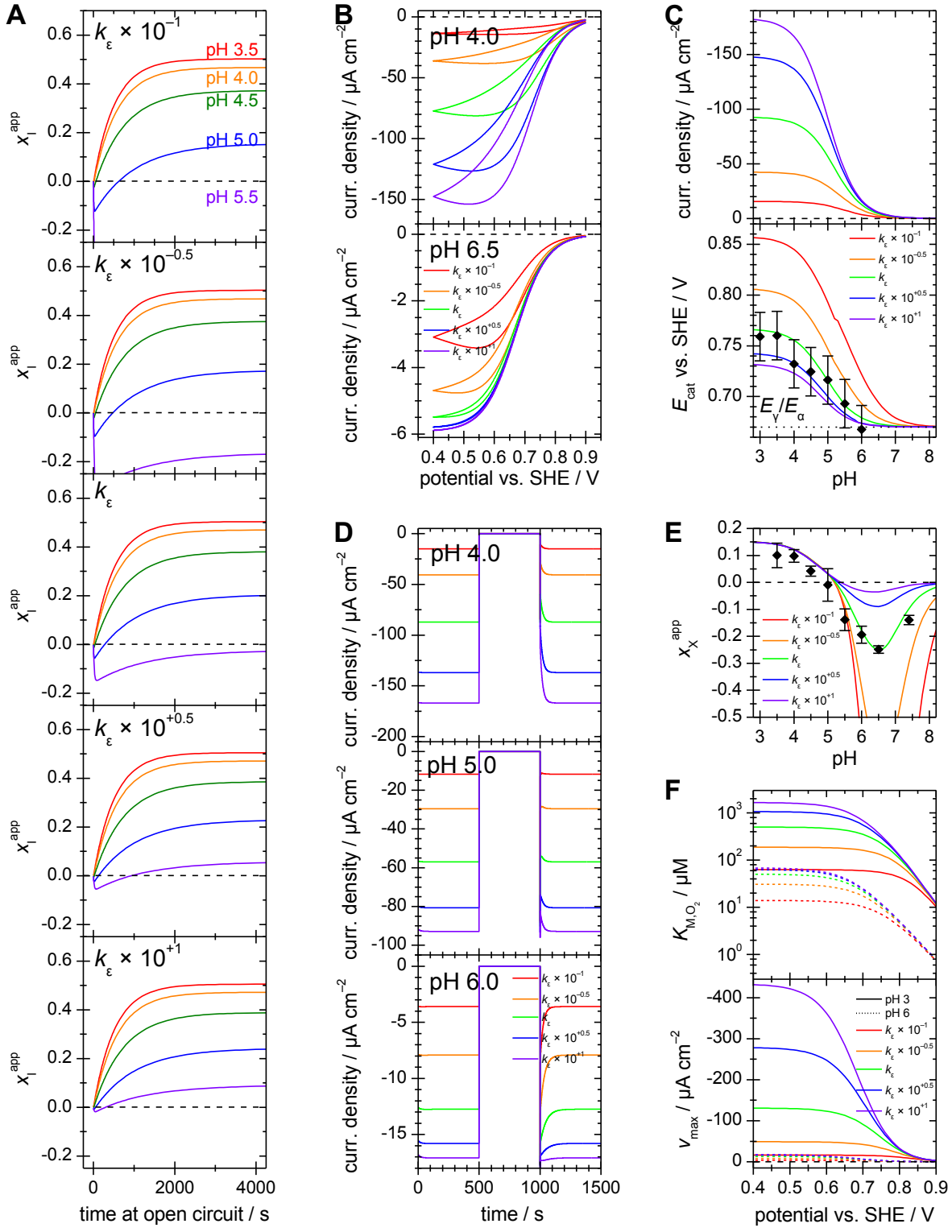

Figure S14. Graphical illustration of the effect of varying k_ε over two orders of magnitude, with the center value (green line in parts B–F) the same as that used in the figures in the main text. With increasing k_ε there is (A) a disappearance of the negative part of the apparent fraction inactivated (x_I^{app}) at higher pH values and longer times at open circuit (cf. Fig. 2B); (B) an increase in catalytic current (first scan, 10 mV s^{-1}, cf. Fig. 7); (C) a marked increase in catalytic activity and decrease in E_{cat} (cf. Fig. 5); (D) a marked increase in steady-state catalytic activity at all pH values, but no change in activation profile (cf. Fig. 8, middle panels); (E) a large decrease in apparent fraction of X State (x_X^{app}) at higher pH values (cf. Fig. 4B); and (F) an increase in $K_{M,O2}$ and v_{max} at both low and high pH values (cf. Fig. 6).

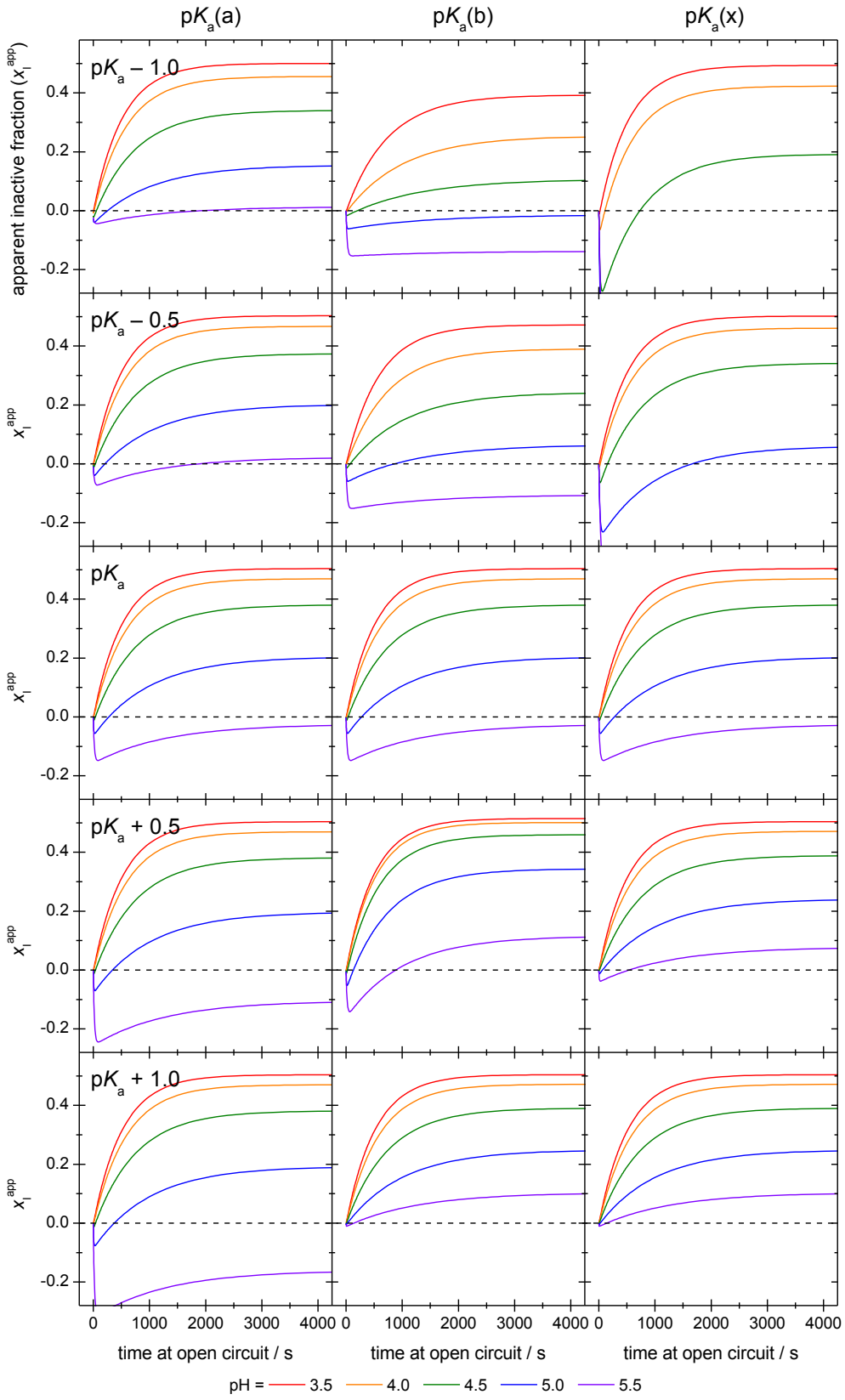

Figure S15. The effect of varying the pK_a values associated with the k_α , k_β and k_{-x} steps on the pH- and time-dependence of the apparent fraction of inactivated enzyme (x_I^{app}) (cf. Fig. 2B). The plots in the middle rows are identical to each other and to the simulation overlay in Fig. 2B.

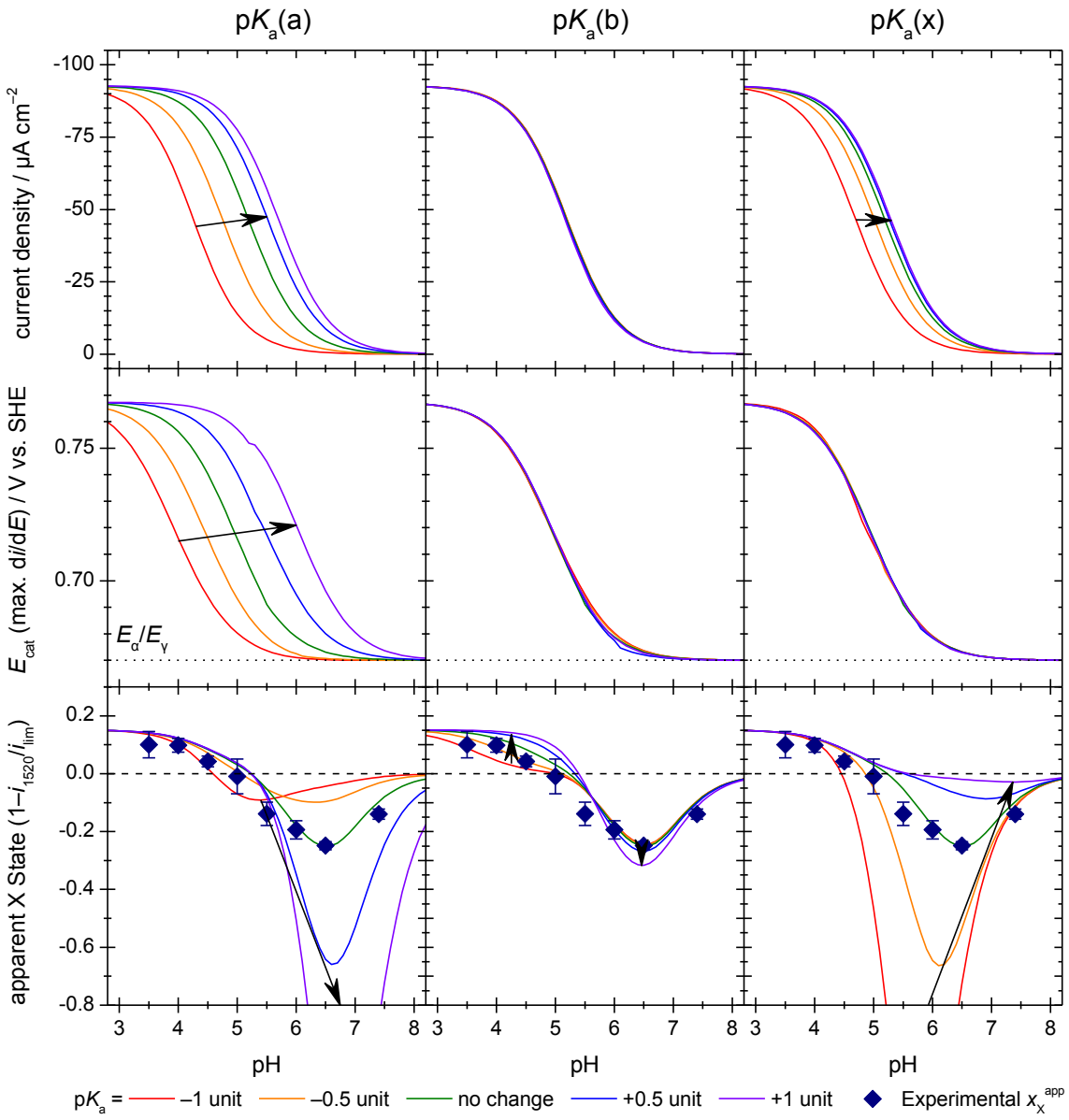

Figure S16. The effect of varying the pK_a values associated with the k_α, k_β and k_{-x} steps on the pH-dependence of: (top row) the steady-state current (i.e., catalytic activity, cf. Fig. 5 inset); (middle row) position of the maximum of the first derivative in the cyclic voltammograms ("E_{cat}", 10 mV s^{-1}, cf. Fig. 5); and (bottom row) the apparent fraction of enzyme in the X State (x_X^{app}) (cf. Fig. 4B). The dotted line in the middle panels indicates the characteristic potential for formation of the Reduced species. The arrows indicate the trend of each plot with an increase in pK_a.

Section S8 Predicted steady fraction of enzyme states

Plots of steady-state fraction of enzyme at open circuit and under an applied potential of 0.4 V vs. SHE shown in Figure S17 can guide experimental conditions required to generate each of the catalytic states (e.g., for spectroscopy or X-ray crystallography) and allow the fractions of other states present under a set of conditions to be predicted.

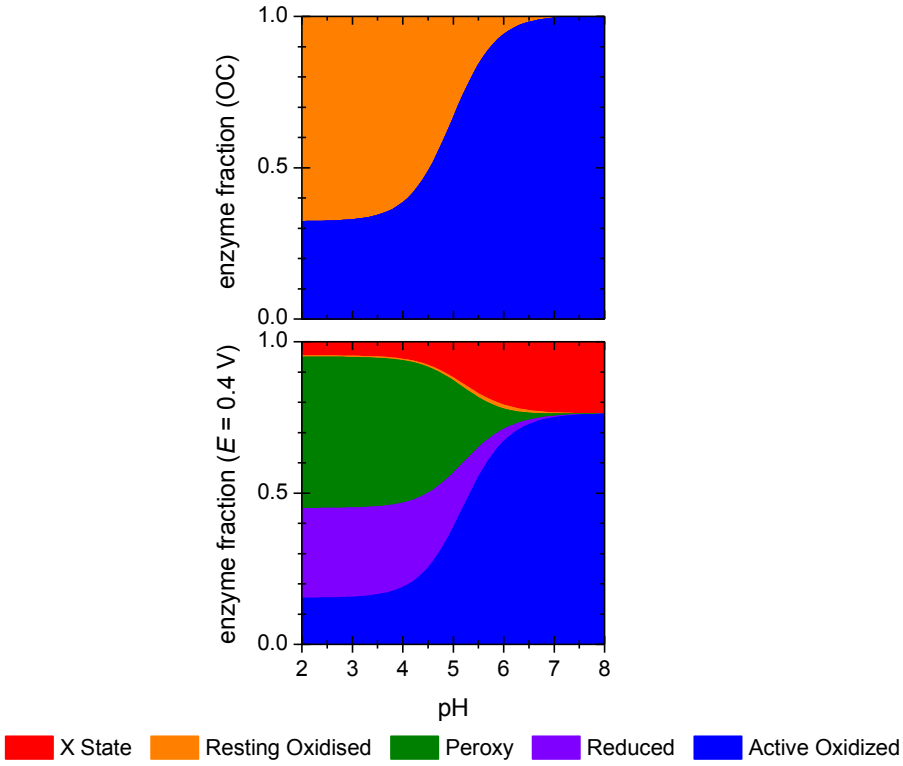

Figure S17. Predicted fractions of each enzyme state as a function of pH, based on the parameters given in Table 1. The top panel shows how the equilibrium shifts between the Resting Oxidized form of the enzyme and the Active Oxidized form. The bottom panel shows the diminishing presence of the Peroxy and Reduced forms of the enzyme with increasing pH, and the concomitant increase in the Active Oxidized form and the X State.

Section S9 Iteration algorithm to find $k_{-\beta}$ and k_{+x}

The values for $k_{-\beta}$ and k_{+x} are determined iteratively based on the apparent fraction of the Resting Oxidized form of the enzyme at pH 3.5 and 5.5 (see Analysis). The iteration scheme is outlined below.

Need

1. Fraction inactivated at lower pH and after a long time at open circuit (x_I^{low}).
2. Fraction inactivated at lower pH and after a long time at open circuit (x_I^{high}), with a known tolerance (σ).[1]
3. Values for $k_\alpha^{max,low\ pH}$, $k_{+\beta}$, k_γ^{max}, k_δ, k_ε, k_{-x}, all pK_a values.
4. Seed value for k_{+x}.

Pseudocode

- Set test parameter (calculated x_I^{high}) to a value outside the acceptance range.
- Set step counter to 0.
- Establish values for all rate constants except $k_{-\beta}$ and k_{+x} at both low and high pH values, adjusted for pH and potential as appropriate.
- Set an initial value for $k_{-\beta}$ based on low pH rate constants and x_I^{low}.[2]
- Iterate until the calculated value of x_I^{high} is within the acceptance range or until a maximum number of steps is reached (in case the values do not converge).
  - Calculate k_{+x} using high-pH rate constants, including $k_{-\beta}$ (e.g., Eqn. S7).
  - Calculate $k_{-\beta}$ using low-pH rate constant, including k_{+x} (e.g., Eqn. S8)
  - Calculate x_I^{high}.
- Return converged $k_{-\beta}$ and k_{+x} or an error flag.

*Sample formulas: "P deadend" kinetic scheme with pH dependence on the formation of the X State (*Figure S4*)*

$$k_{-\beta} = -((x_I^{low}\,(k_\delta\,k_\varepsilon + k_\alpha\,(k_\delta + k_\varepsilon))\,k_\gamma\,k_{-x} + k_{+\beta}\,((2x_I^{low} - 1)\,k_\delta\,k_\varepsilon + (x_I^{low} - 1)\,k_\alpha\,(k_\delta + k_\varepsilon) + x_I^{low}\,(k_\delta + k_\varepsilon)\,k_\gamma)\,k_{-x} + (1 + x_I^{low})\,k_\alpha\,k_\delta\,k_\gamma\,k_{+x} + k_{+\beta}\,k_\delta\,(k_\gamma + x_I^{low}\,(k_\alpha + k_\gamma))\,k_{+x} \pm (-4\,k_{+\beta}\,(x_I^{low}\,(k_\delta\,k_\varepsilon + k_\alpha\,(k_\delta + k_\varepsilon))\,k_{-x} + (1 + x_I^{low})\,k_\alpha\,k_\delta\,k_{+x})\,((x_I^{low} - 1)\,(k_{+\beta}\,k_\delta\,k_\varepsilon + ((k_\alpha + k_{+\beta})\,k_\delta + (k_\alpha + k_{+\beta} + k_\delta)\,k_\varepsilon)\,k_\gamma)\,k_{-x} + x_I^{low}\,(k_\alpha + k_{+\beta})\,k_\delta\,k_\gamma\,k_{+x}) + (((2x_I^{low} - 1)\,k_{+\beta}\,k_\delta\,k_\varepsilon + (x_I^{low} - 1)\,k_\alpha\,k_{+\beta}\,(k_\delta + k_\varepsilon) + x_I^{low}\,((k_\alpha + k_{+\beta})\,k_\delta + (k_\alpha + k_{+\beta} + k_\delta)\,k_\varepsilon)\,k_\gamma)\,k_{-x} + k_\delta\,(x_I^{low}\,k_\alpha\,k_{+\beta} + (1 + x_I^{low})\,(k_\alpha + k_{+\beta})\,k_\gamma)\,k_{+x})^2)^{1/2})/(2x_I^{low}\,(k_\delta\,k_\varepsilon + k_\alpha\,(k_\delta + k_\varepsilon))\,k_{-x} + 2(1 + x_I^{low})\,k_\alpha\,k_\delta\,k_{+x})) \quad \text{(S7)}$$

$$k_{+x} = -(((-k_{+\beta} + x_I^{high}\,(k_{-\beta} + k_{+\beta}))\,((k_{-\beta} + k_{+\beta})\,k_\delta\,k_\varepsilon + (k_\delta\,k_\varepsilon + k_{+\beta}\,(k_\delta + k_\varepsilon))\,k_\gamma + k_\alpha\,(k_\delta + k_\varepsilon)\,(k_{-\beta} + k_\gamma))\,k_{+x})/((k_{-\beta} + x_I^{high}\,k_{-\beta} + x_I^{high}\,k_{+\beta})\,k_\delta\,(k_{+\beta}\,k_\gamma + k_\alpha\,(k_{-\beta} + k_\gamma)))) \quad \text{(S8)}$$

This algorithm is included at the end of all the Matlab routines with the prefix `BMCO_search_` as the function `find_betaback_xforward` (cf. Section S14).

[1] The value of x_I^{low} is fixed, while x_I^{high} has a range of values, reflecting the lower activity and lower inactive fraction of the high pH measurements.

[2] The square-root term in Eqn. S7 means there can be multiple solutions providing values for $k_{-\beta}$, and that negative and imaginary values can result. These are picked up by tests in the iteration loop. Solutions converging to negative values for either $k_{-\beta}$ or k_{+x} are discarded after the search loops.

Section S10 Simulating catalytic voltammetry of surface-bound redox enzymes

Section S10.1 Outline of Honeychurch–Bernhardt finite difference method

There are established methods for providing analytical solutions for systems of first-order differential equations such as those generated in the simulation of reaction kinetics, but the resultant equations tend to be complex and involve sums of exponential terms of greatly varying magnitude, which leads to precision errors when computed. In this publication, we adopted the finite-difference numerical method developed by Honeychurch and Bernhardt (M.J. Honeychurch and P.V. Bernhardt, *J. Phys. Chem. B* 2004, **108,** 15900–15909 and M.J. Honeychurch, *Simulating Electrochemical Reactions with Mathematica;* IBNH: St. Lucia, Queensland, Australia, 2006). We outline their method below then provided a specific example based on the "P deadend" scheme illustrated in Figure S4.

We start with a column vector of the fractions of each enzyme species or form present in our scheme (**b)** and a matrix of (pseudo-)first-order[3] rate constants **K** (that is, the coefficient that appears before the concentration or fraction of each state) to give a system of first-order differential equations:

$$\frac{\mathrm{d}\mathbf{b}}{\mathrm{d}t} = \mathbf{K}\,\mathbf{b} \tag{S9}$$

The operator d/dt in Eqn. S9 is turned into a finite difference form ($\Delta/\Delta t$ operator), and the equations are multiplied through by $RT\Delta t/F\Delta E$ (Eqn. S10). The rate constants in **K** is converted into dimensionless rate constants in **M** by Eqns. S11. The form in S11a is used for simulations of cyclic voltammograms, in which there is a scan-rate dependence, and the form in S11b is used for chronoamperometry simulations.

$$\frac{RT}{F\Delta E}\frac{\mathrm{d}\mathbf{b}}{\mathrm{d}t} = \mathbf{M}\,\mathbf{b} \tag{S10}$$

$$m_i = \frac{RT}{F\upsilon}k_\mathrm{i} \tag{S11a}$$

$$m_i = \frac{RT\Delta t}{F\Delta E}k_\mathrm{i} \tag{S11b}$$

[3] That is, any rate equation including $[O_2]$ or $[H^+]$ has its rate constant transformed into a pseudo-first-order rate constant by incorporating the substrate concentration. For example, $k_\alpha = k_\alpha' [H^+]^a$.

Rearranging, this gives a system of linear equations describing the value for the enzyme fractions at time step n ($\mathbf{b}^n$) as a function of their fractions at time step n+1 ($\mathbf{b}^{n+1}$). A factor $\tau = F\Delta E/RT$ is introduced for CV simulations (Eqn. S12a), this factor is unnecessary for CA simulations (Eqn. S12b):

$$\mathbf{b}^n = (\mathbf{I} - \tau\,\mathbf{M})\,\mathbf{b}^{n+1} \tag{S12a}$$

$$\mathbf{b}^n = (\mathbf{I} - \mathbf{M})\,\mathbf{b}^{n+1} \tag{S12b}$$

where $\mathbf{I}$ is the identity matrix with dimensions matching $\mathbf{M}$. Inverting the matrix provides the expressions needed to calculate enzyme fractions for the next time step from the fractions present at the current one:

$$\mathbf{b}^{n+1} = (\mathbf{I} - \tau\,\mathbf{M})^{-1}\,\mathbf{b}^n \tag{S13a}$$

$$\mathbf{b}^{n+1} = (\mathbf{I} - \mathbf{M})^{-1}\,\mathbf{b}^n \tag{S13b}$$

The expression in each of the cells of the inverse matrix has a common denominator which is factored out to speed up processing.

For the case of the schemes shown in Figure S4, the corresponding matrices and equations are:

$$\mathbf{b} = \begin{bmatrix} x_\mathrm{A} \\ x_\mathrm{R} \\ x_\mathrm{P} \\ x_\mathrm{I} \\ x_\mathrm{X} \end{bmatrix} \tag{S14}$$

where x_N, x_R, x_P, x_I and x_X are, respectively, the Native, Reduced, Peroxy, Resting Oxidized and X State forms of the enzyme.

$$\mathbf{K'} = \begin{bmatrix} -(k_\alpha' [\mathrm{H}^+]^\mathrm{a} + k_{+\beta}' [\mathrm{H}^+]^\mathrm{b}) & 0 & k_\varepsilon' [\mathrm{H}^+]^\mathrm{e} & k_{-\beta} & 0 \\ k_\alpha' [\mathrm{H}^+]^\mathrm{a} & -k_\delta' [\mathrm{H}^+]^\mathrm{d} & 0 & k_\gamma' [\mathrm{H}^+]^\mathrm{g} & 0 \\ 0 & k_\delta' [\mathrm{H}^+]^\mathrm{d} & -(k_\varepsilon' [\mathrm{H}^+]^\mathrm{e} + k_{+\mathrm{x}}) & 0 & k_{-\mathrm{x}}' [\mathrm{H}^+]^\mathrm{x} \\ k_{+\beta}' [\mathrm{H}^+]^\mathrm{b} & 0 & 0 & -(k_{-\beta} + k_\gamma' [\mathrm{H}^+]^\mathrm{g}) & 0 \\ 0 & 0 & k_{+\mathrm{x}} & 0 & -k_{-\mathrm{x}}' [\mathrm{H}^+]^\mathrm{x} \end{bmatrix} \tag{S15}$$

Transforming all the non-first-order rate constants (marked with a prime) into pseudo-first-order rate constants (Eqn. S16), then making them dimensionless by multiplying through by RT/Fv, gives Eqn. S17. Following the process through gives the ($\mathbf{I} - \tau\,\mathbf{M}$) form (Eqn. S18) which will be inverted.

$$\mathbf{K} = \begin{bmatrix} -(k_\alpha + k_{+\beta}) & 0 & k_\varepsilon & k_{-\beta} & 0 \\ k_\alpha & -k_\delta & 0 & k_\gamma & 0 \\ 0 & k_\delta & -(k_\varepsilon + k_{+x}) & 0 & k_{-x} \\ k_{+\beta} & 0 & 0 & -(k_{-\beta} + k_\gamma) & 0 \\ 0 & 0 & k_{+x} & 0 & -k_{-x} \end{bmatrix} \tag{S16}$$

$$\mathbf{M} = \begin{bmatrix} -(m_\alpha + m_{+\beta}) & 0 & m_\varepsilon & m_{-\beta} & 0 \\ m_\alpha & -m_\delta & 0 & m_\gamma & 0 \\ 0 & m_\delta & -(m_\varepsilon + m_{+x}) & 0 & m_{-x} \\ m_{+\beta} & 0 & 0 & -(m_{-\beta} + m_\gamma) & 0 \\ 0 & 0 & m_{+x} & 0 & -m_{-x} \end{bmatrix} \tag{S17}$$

$$(\mathbf{I} - \tau\,\mathbf{M}) = \begin{bmatrix} 1 + \tau\,(m_\alpha + m_{+\beta}) & 0 & -\tau\,m_\varepsilon & -\tau\,m_{-\beta} & 0 \\ -\tau\,m_\alpha & 1 + \tau\,m_\delta & 0 & -\tau\,m_\gamma & 0 \\ 0 & -\tau\,m_\delta & 1 + \tau\,(m_\varepsilon + m_{+x}) & 0 & -\tau\,m_{-x} \\ 1 + \tau\,m_{+\beta} & 0 & 0 & -(m_{-\beta} + m_\gamma) & 0 \\ 0 & 0 & -\tau\,m_{+x} & 0 & 1 + \tau\,m_{-x} \end{bmatrix} \tag{S18}$$

The matrix was inverted (using Mathematica in this case), and the common denominator factored out. The system of equations that arise from Eqns. S19 estimates the fraction of each enzyme state after the next time step, given the set of enzyme states from the previous step. The calculation is simplified in practice because the enzyme fractions must sum to one.

$$D\,(\mathbf{I} - \tau\,\mathbf{M})^{-1} = \begin{bmatrix} (1 + m_\delta\,\tau)\,(1 + m_{-\beta}\,\tau + m_\gamma\,\tau)\,(1 + m_{-x}\,\tau + m_{+x}\,\tau + m_\varepsilon\,\tau\,(1 + m_{-x}\,\tau)) & \cdots \\ \tau\,(m_\alpha + m_\alpha\,m_{-\beta}\,\tau + m_\alpha\,m_\gamma\,\tau + m_{+\beta}\,m_\gamma\,\tau)\,(1 + m_{-x}\,\tau + m_{+x}\,\tau + m_\varepsilon\,\tau\,(1 + m_{-x}\,\tau)) & \cdots \\ m_\delta\,\tau^2\,(m_\alpha + m_\alpha\,m_{-\beta}\,\tau + m_\alpha\,m_\gamma\,\tau + m_{+\beta}\,m_\gamma\,\tau)\,(1 + m_{-x}\,\tau) & \cdots \\ m_{+\beta}\,\tau\,(1 + m_\delta\,\tau)\,(1 + m_{-x}\,\tau + m_{+x}\,\tau + m_\varepsilon\,\tau\,(1 + m_{-x}\,\tau)) & \cdots \\ m_\delta\,m_{+x}\,\tau^3\,(m_\alpha + m_\alpha\,m_{-\beta}\,\tau + m_\alpha\,m_\gamma\,\tau + m_{+\beta}\,m_\gamma\,\tau) & \cdots \end{bmatrix} \tag{S19a}$$

$$\begin{aligned} D = {} & -m_{-x}\,m_x\,\tau^2\,(1 + m_\delta\,\tau)\,(1 + m_\alpha\,\tau + m_{-\beta}\,\tau + m_{+\beta}\,\tau + m_\gamma\,\tau + m_\alpha\,m_{-\beta}\,\tau^2 + m_\alpha\,m_\gamma\,\tau^2 + m_{+\beta}\,m_\gamma\,\tau^2) + \\ & (1 + m_{-x}\,\tau)\,(m_{+\beta}\,\tau\,(-m_\delta\,m_\varepsilon\,m_\gamma\,\tau^3 - (1 - (-m_\varepsilon - m_{+x})\,\tau)\,(m_{-\beta}\,\tau + m_{-\beta}\,m_\delta\,\tau^2)) + \\ & (1 - (-m_{-\beta} - m_\gamma)\,\tau)\,(-m_\alpha\,m_\delta\,m_\varepsilon\,\tau^3 + (1 - (-m_\varepsilon - m_{+x})\,\tau)\,(1 + m_\alpha\,\tau + m_{+\beta}\,\tau + m_\delta\,\tau + m_\alpha\,m_\delta\,\tau^2 + \\ & m_{+\beta}\,m_\delta\,\tau^2))) \end{aligned} \tag{S19b}$$

Section S10.2 Steady-state equations

In contrast to the results of the finite-difference modeling, determination of the steady-state fractions of different enzyme states produces simple expressions that are readily calculated from linear algebra. We used these expressions to provide a starting point for the voltammetry simulations that experimentally began with a long period held at a specific potential or at open circuit.

In brief, we begin with the mathematically over-determined system of equations

$$\frac{\mathrm{d}\mathbf{b}}{\mathrm{d}t} = \mathbf{K}\,\mathbf{b} = \mathbf{0} \tag{S20}$$

where $\mathbf{0}$ is a column vector in which all the elements are zero, then create a modified version of the matrix of rate equations ($\mathbf{K}_{ss}$) in which each cell in one line has the contents replaced by 1 to include a mass balance, giving Eqn. S21a, which can be solved with the inverse matrix of $\mathbf{K}_{SS}$ (Eqn. S21b). The result is further simplified for open-circuit cases in which k_α and k_γ are zero and the only species present are the Active Oxidized form and the Resting Oxidized forms.

$$\mathbf{K}_{SS}\,\mathbf{b} = \begin{bmatrix} 1 \\ 0 \\ 0 \\ 0 \\ 0 \end{bmatrix};\ \mathbf{b} = \mathbf{K}_{SS}^{-1} \begin{bmatrix} 1 \\ 0 \\ 0 \\ 0 \\ 0 \end{bmatrix} \tag{S21}$$

Again, applying the scheme shown in Figure S4 as an example:

$$\mathbf{K}_{SS} = \begin{bmatrix} 1 & 1 & 1 & 1 & 1 \\ k_\alpha & -k_\delta & 0 & k_\gamma & 0 \\ 0 & k_\delta & -(k_\varepsilon + k_x) & 0 & k_{-x} \\ k_{+\beta} & 0 & 0 & -(k_{-\beta} + k_\gamma) & 0 \\ 0 & 0 & k_x & 0 & -k_{-x} \end{bmatrix} \tag{S22}$$

$$\mathbf{K}_{SS}^{-1} = \frac{1}{D_{SS}} \begin{bmatrix} k_\delta\,k_\varepsilon\,(k_{-\beta}+k_\gamma)\,k_{-x} & (k_{-\beta}+k_\gamma)\,(k_\varepsilon\,k_{-x}+k_\delta\,(k_{-x}+k_x)) & k_\delta\,(k_{-\beta}+k_\gamma)\,(k_{-x}+k_x) \\ k_\varepsilon\,(k_{+\beta}\,k_\gamma+k_\alpha\,(k_{-\beta}+k_\gamma))\,k_{-x} & (-k_\varepsilon)\,(k_{-\beta}+k_{+\beta}+k_\gamma)\,k_{-x} & (k_{+\beta}\,k_\gamma+k_\alpha\,(k_{-\beta}+k_\gamma))\,(k_{-x}+k_{+x}) \\ k_\delta\,(k_{+\beta}\,k_\gamma+k_\alpha\,(k_{-\beta}+k_\gamma))\,k_{-x} & (-k_\delta)\,(k_{-\beta}+k_{+\beta}+k_\gamma)\,k_{-x} & (-(k_{-\beta}\,k_\delta+k_{+\beta}\,k_\delta+k_{+\beta}\,k_\gamma+k_\delta\,k_\gamma+k_\alpha\,(k_{-\beta}+k_\gamma)))\,k_{-x} \\ k_{+\beta}\,k_\delta\,k_\varepsilon\,k_{-x} & k_{+\beta}\,(k_\varepsilon\,k_{-x}+k_\delta\,(k_{-x}+k_{+x})) & k_\beta\,k_\delta\,(k_{-x}+k_{+x}) \\ k_\delta\,(k_\beta\,k_\gamma+k_\alpha\,(k_{-\beta}+k_\gamma))\,k_{+x} & (-k_\delta)\,(k_{-\beta}+k_{+\beta}+k_\gamma)\,k_{+x} & (-(k_{-\beta}\,k_\delta+k_{+\beta}\,k_\delta+k_{+\beta}\,k_\gamma+k_\delta\,k_\gamma+k_\alpha\,(k_{-\beta}+k_\gamma)))\,k_{+x} \end{bmatrix}$$

$$\begin{bmatrix} k_\varepsilon\,k_\gamma\,k_{-x}+k_\delta\,(k_\varepsilon\,k_{-x}+k_\gamma\,(k_{-x}+k_{+x})) & k_\delta\,(k_{-\beta}+k_\gamma)\,(k_\varepsilon+k_{-x}+k_{+x}) \\ k_\varepsilon\,(k_\alpha-k_\gamma)\,k_{-x} & (k_{+\beta}\,k_\gamma+k_\alpha\,(k_{-\beta}+k_\gamma))\,(k_\varepsilon+k_{-x}+k_{+x}) \\ k_\delta\,(k_\alpha-k_\gamma)\,k_{-x} & k_\alpha\,(k_{-\beta}+k_\gamma)\,(k_\delta-k_{-x})-k_\delta\,(k_{-\beta}+k_\gamma)\,k_{-x}+k_{+\beta}\,(k_\delta\,k_\gamma-k_\delta\,k_{-x}-k_\gamma\,k_{-x}) \\ -k_\delta\,k_\varepsilon\,k_{-x}-k_\alpha\,(k_\varepsilon\,k_{-x}+k_\delta\,(k_{-x}+k_{+x})) & k_{+\beta}\,k_\delta\,(k_\varepsilon+k_{-x}+k_{+x}) \\ k_\delta\,(k_\alpha-k_\gamma)\,k_{+x} & -(k_\beta\,(k_\gamma\,(k_\delta+k_\varepsilon+k_{+x})+k_\delta\,(k_\varepsilon+k_{+x}))+k_\delta\,k_\gamma\,(k_\varepsilon+k_{+x})+k_{-\beta}\,k_\delta\,(k_\varepsilon+k_{+x})+k_\alpha\,(k_{-\beta}+k_\gamma)\,(k_\delta+k_\varepsilon+k_{+x})) \end{bmatrix} \tag{S23}$$

$$\mathbf{b} = \begin{bmatrix} x_A \\ x_R \\ x_P \\ x_I \\ x_X \end{bmatrix} = \frac{1}{D_{SS}} \begin{bmatrix} k_\delta\, k_\varepsilon\, (k_{-\beta} + k_\gamma)\, k_{-x} \\ k_\varepsilon\, (k_{+\beta}\, k_\gamma + k_\alpha\, (k_{-\beta} + k_\gamma))\, k_{-x} \\ k_\delta\, (k_{+\beta}\, k_\gamma + k_\alpha\, (k_{-\beta} + k_\gamma))\, k_{-x} \\ k_\beta\, k_\delta\, k_\varepsilon\, k_{-x} \\ k_\delta\, (k_{+\beta}\, k_\gamma + k_\alpha\, (k_{-\beta} + k_\gamma))\, k_{+x} \end{bmatrix} \quad \text{(S24a)}$$

$$D_{SS} = ((k_{-\beta} + k_{+\beta})\, k_\delta\, k_\varepsilon + (k_\delta\, k_\varepsilon + k_{+\beta}\, (k_\delta + k_\varepsilon))\, k_\gamma)\, k_{-x} + k_{+\beta}\, k_\delta\, k_\gamma\, k_{+x} + k_\alpha\, (k_{-\beta} + k_\gamma)\, (k_\varepsilon\, k_{-x} + k_\delta\, (k_{-x} + k_{+x})) \quad \text{(S24b)}$$

And for open circuit

$$\mathbf{b} = \begin{bmatrix} x_N \\ x_R \\ x_P \\ x_I \\ x_X \end{bmatrix} = \frac{1}{k_{+\beta} + k_{-\beta}} \begin{bmatrix} k_{-\beta} \\ 0 \\ 0 \\ k_{+\beta} \\ 0 \end{bmatrix} \quad \text{(S25)}$$

Section S11 Extended derivations

All the mathematical relationships that relate to our primary observable, catalytic current, are based on Eqn. S26 which takes the rates of the two steps in the catalytic scheme that involve interfacial electron transfer, weights them by their relative fractions, then converts that into catalytic current density.

$$i_{cat} = -\,n\,F\,\Gamma_{total}\,(k_\alpha\,x_A + k_\gamma\,x_I) \tag{S26}$$

where n is the number of electrons per catalytic cycle (i.e., per molecule of O_2), F is Faraday's constant, and x_A and x_I are the respective fractions of the Active Oxidized form and the Resting Oxidized form of the enzyme, and Γ_{total} is the surface concentration of catalytically competent enzyme.

The potential for the maximum change in current density with change in potential (i.e., di/dE) is E_{cat}. We assume that the potential sweep rate is small enough that a steady-state approximation applies and that the contribution from the reduction of the Resting Oxidized form is negligible. The fraction of enzyme in the Active Oxidized form is given by Eqns. S25 (cf. Eqn. S37). The value for k_α depends on both applied potential (Eqn. S27) and pH (Eqn. S28).

$$k_\alpha(E_{applied}) = \frac{k_\alpha^{\,max}}{1 + \exp[F\,(E_{applied} - E_{ET})\,\alpha/RT]} \tag{S27}$$

$$k_\alpha(\mathrm{pH}) = k_\alpha^{\,low\ pH}\left(1 - \frac{1}{1 + 10^{pK_a(a)-pH}}\right) \tag{S28}$$

where $E_{applied}$ is the electrode potential, E_{ET} is the characteristic potential associated with interfacial electron transfer, α is the dimensionless charge transfer coefficient, R is the gas constant, T is absolute temperature, and pK_a(a) is the pK_a associated with the proton-dependency of the reduction of the Active Oxidized form (Section S5).

Substituting Eqn. S27 into Eqn. S26, taking the derivative with respect to $E_{applied}$ and eliminating the smaller terms gives Eqn. S29.

$$E_{cat} \approx E_\alpha + \frac{R\,T}{\alpha\,F}\ln\frac{k_\alpha^{\,max}(\mathrm{pH}) + k_\varepsilon}{k_\varepsilon} \tag{S29}$$

where $k_\alpha^{\,max}$(pH) denotes that this is the maximum rate for the specified pH. Substituting in Eqn. S29 then rearranging gives Eqn. S30, which provides a value for E_{cat} at any pH value.

$$E_{cat} = E_{\alpha} + \frac{R\,T}{\alpha\,F} \ln\left[1 + \frac{{k_{\alpha}}^{\text{max low pH}}}{k_{\varepsilon}} \frac{10^{pKa}}{10^{pKa} + 10^{pH}}\right] \tag{S30}$$

We can derive a simple expression for the range in E_{cat} values by looking at the limits where pH→–∞ and pH→+∞ (Eqn. S31).

$$\Delta(E_{cat}) = \frac{R\,T}{\alpha\,F} \ln \frac{{k_{\alpha}}^{\text{max low pH}} + k_{\varepsilon}}{k_{\varepsilon}} \tag{S31}$$

Taking the derivative of Eqn. S30, setting the result to zero and solving for pH gives the inflection point for the resultant sigmoid (Eqn. S32), which is shifted from the associated pK_a value because of the influence of kinetics on the value for E_{cat}. Substituting this pH value back into the derivative gives the maximum slope in E_{cat} vs. pH (Eqn. S33). When ${k_{\alpha}}^{\text{max low pH}} \to \infty$ or $k_{\varepsilon} \to 0$, the slope reaches its maximum of $-\ln(10)\,RT/\alpha F$. When $k_{\varepsilon} >> {k_{\alpha}}^{\text{max low pH}}$, the slope approaches zero.

$$pK_a^{\text{app}} = pK_a(a) + \frac{1}{2} \log_{10}\left(\frac{{k_{\alpha}}^{\text{max low pH}} + k_{\varepsilon}}{k_{\varepsilon}}\right) \tag{S32}$$

$$\left.\frac{dE_{cat}}{d(pH)}\right|^{\text{max}} = -\ln(10)\,\frac{R\,T}{\alpha\,F}\left[1 - \frac{2\,k_{\varepsilon}}{{k_{\alpha}}^{\text{max low pH}}}\left(\sqrt{\frac{{k_{\alpha}}^{\text{max low pH}} + k_{\varepsilon}}{k_{\varepsilon}}} - 1\right)\right] \tag{S33}$$

The rate constants $k_{+\beta}$ and $k_{-\beta}$ were calculated from a first-order differential equation (Eqn. S34) that assumes that only the Native and Resting Oxidized states are present in the system (that is, the other states decay quickly enough that they can be ignored after the applied potential ceases).

$$\frac{dx_I}{dt} = k_{+\beta}\,x_A - k_{-\beta}\,x_I = k_{+\beta}\,(1 - x_I) - k_{-\beta}\,x_I \tag{S34}$$

Assuming that at $t = 0$ the fraction of Resting Oxidized is zero, the definite integral is Eqn. S35 which can be fit by a non-linear least squares method:

$$\exp(-t/\tau_{\beta}) = 1 - \frac{x_I}{k_{-\beta}\,\tau_{\beta}} = k_{+\beta}\,(1 - x_I) - k_{-\beta}\,x_I \tag{S35}$$

where the time constant is given by $\tau_{\beta} = (k_{+\beta} + k_{-\beta})^{-1}$ and the fraction of Resting Oxidized at infinite time at open circuit by ${x_I}^{\infty} = k_{+\beta}\,\tau_{\beta}$. These can be re-arranged to give the rate constants in terms of τ_{β} and ${x_I}^{\infty}$ (Eqns. S36):

$$\left.\begin{aligned} k_{+\beta} &= \frac{{x_I}^{\infty}}{\tau_{\beta}} \\ k_{-\beta} &= \frac{1 - {x_I}^{\infty}}{\tau_{\beta}} \end{aligned}\right\} \tag{S36}$$

Three rate constants describe the main cycle of catalytic O_2 reduction (Scheme 1 in the main text): k_α, which depends on pH and potential; k_δ, which scales linearly with O_2 concentration; and k_ε, which is independent of pH, potential and O_2 concentration. During steady-state turnover, the fraction of the Resting Oxidized state is always less than 1.25% and $k_\gamma << k_\alpha$. Therefore, k_δ and k_ε can be calculated directly from an analysis of the current magnitude as a function of O_2 concentration under conditions where $k_\alpha \rightarrow k_\alpha^{\text{max low pH}}$ — i.e., lower pH values and a strong driving force for reduction (low E_{applied}).

To generate more easily usable equations, Eqn. S26 was simplified by disregarding the contribution to the catalytic current from the reduction of the Resting Oxidized form, and assuming steady-state conditions gives an expression for the current (i_{SS}) as a function of partial pressure of O_2 (Eqn. S37).

$$i_{SS} = -n\,F\,\Gamma_{total}\,k_\alpha\,x_A = -n\,F\,\Gamma_{total} \times \frac{k_\delta\,P\,(k_\alpha\,k_\varepsilon\,(k_{-\beta}+k_\gamma)\,k_{-x})}{k_\varepsilon\,(k_\alpha\,(k_{-\beta}+k_\gamma)+k_{+\beta}\,k_\gamma)\,k_{-x}+k_\delta\,P\,(((k_{-\beta}+k_{+\beta})\,k_\varepsilon+(k_{+\beta}+k_\varepsilon)\,k_\gamma)\,k_{-x}+k_{+\beta}\,k_\gamma\,k_{+x}+k_\alpha\,(k_{-\beta}+k_\gamma)\,(k_{-x}+k_{+x}))} \quad \text{(S37)}$$

where $P = p_{O2}/p^\circ$, and the rate of k_δ assumes $P = 1$. Under limiting conditions (denoted with the superscript "lim") where the pH is at its optimum value, $k_\alpha^{\text{max low pH}} >> k_\varepsilon$ and $E_{\text{applied}} << E_\alpha$, the equation simplifies to

$$i_{SS}^{\text{lim}} = -n\,F\,\Gamma_{total}\,\frac{P\,k_\delta\,k_\varepsilon}{P\,k_\delta + k_\varepsilon} = -n\,F\,\Gamma_{total}\,k_{cat}^{obs} \quad \text{(S38)}$$

The maximum rate for any combination of pH and applied potential can be calculated by calculating the limit when $P \rightarrow \infty$ (i.e., infinite concentration of O_2) under all conditions (Eqn. S39) and under limiting conditions (Eqn. S40).

$$i_{max} = -n\,F\,\Gamma_{total}\,\frac{k_\alpha\,k_\varepsilon\,(k_{-\beta}+k_\gamma)\,k_{-x}}{((k_{-\beta}+k_{+\beta})\,k_\varepsilon+(k_{+\beta}+k_\varepsilon)\,k_\gamma)\,k_{-x}+k_{+\beta}\,k_\gamma\,k_{+x}+k_\alpha\,(k_{-\beta}+k_\gamma)\,(k_{-x}+k_{+x})} \quad \text{(S39)}$$

$$i_{max}^{\text{lim}} = -n\,F\,\Gamma_{total}\,k_\varepsilon \quad \text{(S40)}$$

The Michaelis-Menten constant is equal to the concentration of substrate in solution that produces half the maximum rate, leading to Eqn. S41 for the general solution and Eqn. S42 for the limiting case.

$$K_{M\text{-}O2} = k_H\,\frac{k_\varepsilon\,(k_\alpha\,(k_{-\beta}+k_\gamma)+k_{+\beta}\,k_\gamma)\,k_{-x}}{k_\delta\,(((k_{-\beta}+k_{+\beta})\,k_\varepsilon+(k_{+\beta}+k_\varepsilon)\,k_\gamma)\,k_{-x}+k_{+\beta}\,k_\gamma\,k_{+x}+k_\alpha\,(k_{-\beta}+k_\gamma)\,(k_{-x}+k_{+x}))} \quad \text{(S41)}$$

$$K_{M\,O_2}^{\text{lim}} = k_H\,p^\circ\,\frac{k_\alpha\,k_\varepsilon}{k_\delta\,(k_\alpha+k_\varepsilon)} \approx k_H\,p^\circ\,\frac{k_\varepsilon}{k_\delta} \quad \text{(S42)}$$

where k_H is the Henry's law constant for O_2 in water, ca. 1.2 mM bar^{-1} at 25 °C.

The ratio of Eqn. S39 and Eqn. S41 gives the catalytic efficiency (Eqn. S43), which is predicted to be constant regardless of pH, p_{O2} and applied potential. This equation offers an alternative route to calculating k_δ that is independent of k_ε. Eqn. S43 also implies that the efficiency of MCOs is predominantly determined by the rate at which O_2 binds to the Reduced form.

$$i_{max}/K_{M,O2} \approx -n\,F\,\Gamma_{total}\,\frac{k_\delta}{p^\circ\,k_H} \tag{S43}$$

Under conditions of low pH and low $E_{applied}$, and with a k_{cat} value per enzyme molecule determined from non-turnover signal and limiting catalytic current at a given pressure, rearrangements of Eqns. S38 and S42 give the solution for the rate constants k_δ and k_ε:

$$k_\delta = k_{cat}^{obs}\,\frac{k_H\,p + K_{M\,O_2}\,p^\circ}{K_{M\,O_2}\,p} \tag{S44}$$

$$k_\varepsilon = \frac{K_{M\,O_2}}{k_H\,p^\circ}\,k_\delta \tag{S45}$$

Our mathematical analysis of O_2 binding and its consistency with experimental determinations suggests that binding of O_2 to the reduced enzyme is effectively irreversible under most experimental conditions, with the rate of subsequent conversion (k_ε) being much larger than any rate of dissociation. The simplified Michaelis constant from Eqn. S42 still produces hyperbolic plots of rate vs. substrate concentration. In our measurements at higher potentials (reduced driving force), the enzyme efficiency drops to zero (Fig. 6B); our assumption of irreversible binding may break down under these conditions.

The pH-dependent rate k_{-x} can be estimated from the experimental data at the pH value at which there is a match between the steady-state population of the X State when a potential is applied and the steady-state population of the Resting Oxidized state when the system is at open circuit (Eqn. S46). This pair of steady-state rate equations (cf. Eqns. S25) simplifies to Eqn. S47, which relates k_{-x} to previously determined rate constants.

$$x_I\,(\text{steady-state, open circuit}) = x_X\,(\text{steady-state, } E_{applied}) \tag{S46}$$

$$\frac{k_{+\beta}}{k_{+\beta} + k_{-\beta}} = \frac{k_{\delta}}{k_{\delta} + k_{\varepsilon}} \frac{k_{+x}}{k_{-x}} \tag{S47}$$

The full expression for this calculation, which accounts for the two different pH dependencies, is given in Eqn. S48:

$$k_{-x}^{\text{low pH}} = k_{+x} \left(1 + 10^{\text{pH}-\text{p}K_a(x)}\right) \frac{k_{\delta}}{k_{\delta} + k_{\varepsilon}} \left[1 + \frac{k_{-\beta}}{k_{+\beta}^{\text{low pH}}} \left(1 + 10^{\text{pH}-\text{p}K_a(b)}\right)\right] \tag{S48}$$

Identical results (except for a scaling factor) can be generated with either a $[H^+]^{-1}$ dependence on the k_{+x} step or a $[H^+]^1$ dependence on the reverse step; the latter is chemically relevant and implicates the ionization of a weakly acidic group.

Section S12 Selection of "P deadend" model over "P bridge"

Studies of the decay of the Reduced and Peroxy Intermediates of laccase from *Rhus vernicifera* have shown some apparently contradictory results that not only can be explained by our modeling, but also helped us select a final kinetic scheme. The work of Palmer and co-workers (*J. Am. Chem. Soc.* 2001, **123,** 6591–6599), building on work from Shin and co-workers (*J. Am. Chem. Soc.* 1996, **118,** 3202–3215), presents extensive rate analyses based on stopped-flow measurements at different pH values for laccase with a fully complement of copper atoms and laccase in which the T1 copper has been substituted with mercury (T1Hg). They observed *no* pH dependence or H/D kinetic isotope effect (KIE) on rate for the formation of the Peroxy or Active Oxidized forms from the Reduced form of the fully competent laccase, but they observed a pH dependence for the depletion of the Peroxy form in the T1Hg laccase. The authors model this decay as two pathways, a faster route requiring a proton from a weak acid and a 10-fold slower route that does not.

We were able to reproduce their observations for the formation of P and A from R using either the "P deadend" or "P bridge" schemes. Significantly, when applying the Honeychurch finite-time step method to truncated and simplified kinetic schemes consisting only of the P, X and A states, only the "P deadend" model was able to reproduce the rate vs. pH sigmoid.

For our simulations of the P to A transition, we began with an equilibrium fractions of the P and X States. The P state was rapidly depleted directly to the A state with no pH dependence, but the slower subsequent depletion the X State showed the sigmoidal rate dependence built into our model. This slower rate dominated the fit to first-order decay kinetics. The center position of the sigmoid shifts to higher pH values. The magnitude of the shift depends on the relative values of the three rate constants. This shift may explain why their apparent pK_a value for the transition is high for aspartate and glutamate side chains.

The equations used to calculate the fraction of P as a function of time are shown below, and were calculated by the method outlined in Section S10. Whereas the expressions for the fraction of P in the "P deadend" scheme (Eqns. S49–S51) involve the pH-dependent rate variables k_{-x}/m_{-x}, those for the "P bridge" scheme (Eqns. S52–S54) do not. This comparison is summarized in Table S1.

"P deadend" scheme

$$\left.\begin{aligned} x_P^{\,0} &= \frac{k_{-x}}{k_{+x} + k_{-x}} \\ x_X^{\,0} &= \frac{k_{+x}}{k_{+x} + k_{-x}} \end{aligned}\right\} \tag{S49}$$

$$\left.\begin{aligned} \frac{dx_P}{dt} &= -(k_\varepsilon + k_{+x})\, x_P + k_{-x}\, x_X \\ \frac{dx_X}{dt} &= k_{+x}\, x_P - k_{-x}\, x_X \end{aligned}\right\} \tag{S50}$$

$$\left.\begin{aligned} x_P^{\,n+1} &= \frac{(1 + m_{-x})\, x_P^{\,n} + m_{-x}\, x_X^{\,n}}{1 + m_\varepsilon + m_{+x} + m_{-x} + m_\varepsilon\, m_{-x}} \\ x_X^{\,n+1} &= \frac{m_{+x}\, x_P^{\,n} + (1 + m_\varepsilon + m_{+x})\, x_X^{\,n}}{1 + m_\varepsilon + m_{+x} + m_{-x} + m_\varepsilon\, m_{-x}} \end{aligned}\right\} \tag{S51}$$

"P bridge" scheme

$$x_P^{\,0} = 1 \tag{S52}$$

$$\frac{dx_P}{dt} = -(k_\varepsilon + k_{+x})\, x_P \tag{S53}$$

$$x_P^{\,n+1} = \frac{1}{1 + m_\varepsilon + m_{+x}}\, x_P^{\,n} \tag{S54}$$

Table S1. A comparison of the pH dependence of the decay rate of the Peroxy Intermediate form if the X State decays to the Active Oxidized form (P bridge) and if it reforms the Peroxy Intermediate (P deadend). To simulate the effect of the mercury substitution of the T1 copper, the conversion rate from Peroxy to Active Oxidized (k_ε) is set 10^5 times lower.

Step from Palmer et al.	P bridge simulation	P deadend simulation
Dithionite reduction	All *Rv*L is in Reduced form.	All *Rv*L is in Reduced form.
Exposure to O_2	*Rv*L forms Peroxy Intermediate.	*Rv*L forms Peroxy Intermediate.
Monitoring decay of P	Peroxy Intermediate forms an Active Oxidized form and the Peroxy Intermediate forms the "X State" (X); neither step has pH dependence.	Peroxy Intermediate equilibrates with "X State" (*pH dependent*) at the same time as the Peroxy Intermediate forms an Active Oxidized form (pH independent).
	The X State then forms an Active Oxidized form (a pH-dependent transformation), but only the Peroxy Intermediate is monitored, so *no pH dependence is observed.*	The remaining "buffer" of X State reforms Peroxy Intermediate at a *pH-dependent rate*, which decays to an Active Oxidized form.

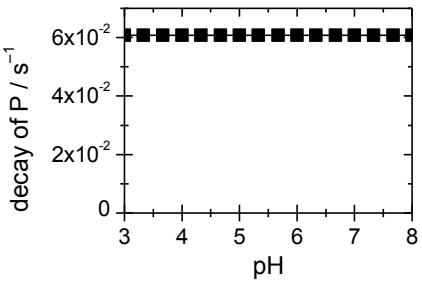

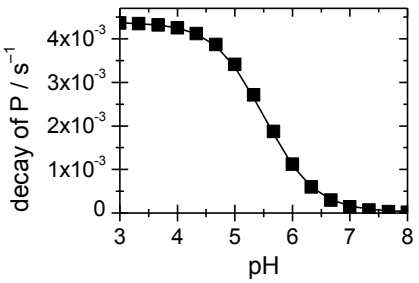

Section S13 Search method used and tests applied to find parameters that fit experimental data

Kinetic models were tested against experimental data by applying a set of "brute force" grid searches. The seed values used in the initial searches were calculated as described in the main text. All the seed values are listed in Table S2.

In the initial grid search, the variables with values set based on published rate constants were fixed. The values of $k_{-\beta}$ and k_x were calculated based on the algorithm described in Section S9. The remaining four variables were changed by at least a factor of 100 in five evenly spaced steps per power of 10 (Table S3); the range of values tested for the "A deadend" searches were increased by another order of magnitude.

Table S2. Center values for each variable in initial searches. The center values depend on whether the proton concentration dependence was assigned to the formation or consumption of the X State. The center value for k_β varies with pH and the order of that reaction with respect to proton concentration.

Variable	Value
$k_\alpha^{\text{max,low pH}}$	2.2×10^{3}
$k_{+\beta}^{\text{low pH}}$	1.0×10^{-3}
$k_{-\beta}$	calculated
k_γ^{max}	5.0×10^{-2}
k_δ	8.1×10^{2} (fixed)
k_ε	4.8×10^{2} (fixed)
k_{+x}	calculated
k_{-x}^{low} pH	7.4×10^{-1}
pK_a(a)	4.5 (fixed)
pK_a(b)	4.5 (fixed)
pK_a(x)	4.5 (fixed)
E_α	0.67 (fixed)
E_γ	0.67 (fixed)

Table S3. Range and increment multiples for searches.

Search	Range	Increment
Initial search 1[a]	$\times 10^{\pm 2}$	$\times 10^{\pm(1/5)} \approx 1.58$
Initial search 2[a]	$\times 10^{\pm 3}$	$\times 10^{\pm(1/5)} \approx 1.58$
Refined search	$\times 10^{\pm(3/5)} \approx 4$	$\times 10^{\pm(1/20)} \approx 1.12$

[a] "Initial search 1" was applied to the schemes in which the X State was generated from the Peroxy Intermediate (see Figure S4 and Figure S5). The wider "Initial search 2" was applied to the schemes in which the X State was generated from the Active Oxidized form (Figure S6).

We defined a set of "wide" and "narrow" criteria to determine whether a set of rate constants matched the experimental data (i.e., a "hit"). The criteria that defined the wide tolerance were based on our empirical fits to our measurements using the "P deadend" scheme Figure S4, then expanded by varying each of the four independent variables by 10±0.5. The boundaries for the tests were based on

the outlier test values, rounded to two significant figures to provide the most generous window. The narrow tolerance criteria were based solely on experimental measurements. When an error bar at one standard deviation was given, its range was doubled to approximate a 95% confidence limit. When range of values was given, this range was expanded by ~1.5 to 2 times to set the limits of acceptable values. A summary of the tests to experimental data are listed in Table S4 as tests 1–8. Tests 9–11 are respectively based on getting converged, positive, non-imaginary values for both $k_{-\beta}$ and k_{+x} from the iterative solutions.

None of the parameters explored in the extended search ranges for the "A deadend" scheme Figure S6) matched the results according to "wide tolerance" criteria. For comparison, we typically found matches based on the *narrower* criteria to the experimental data for the other two schemes over a range of values for each of the variables of greater than an order of magnitude, and typically found about 100 times more hits using the wide criteria. We therefore concluded that the "A deadend" scheme could not reproduce the experimental data and was not a valid model.

We refined our hits from the initial searches with the narrow criteria. The geometric mean of the values that satisfied the "narrow tolerance" selection criteria (Table S4) were used as center/seed values of the refined search range (Table S7 and Table S8) (20 evenly spaced points per order of magnitude for each variable). The hits that resulted from this refined search allowed us to set the acceptable ranges for each of the variables with a precision of about 12%.

All the successful searches are summarized in Section S15.3.

Table S4. Tests applied in search for fits to data listed in order they were applied. Test numbers relate to summaries in Section S15 and Section S15.3.3, and the Matlab simulations in Section S14.

Test	Description	Test expression	Wide tolerance range	Narrow tolerance range
Test 9	$k_{-\beta}$ & k_{-x} do not converge within 200 iterations	$\frac{x_I(\text{SSOC})}{x_X(\text{SS})}$	–0.01 to 0.01 @ pH 5.5*	Same
Test 10	$k_{-\beta}$ or k_{-x} is negative	$k_{-\beta}$ or k_{-x}	> 0	Same
Test 11	$k_{-\beta}$ or k_{-x} is imaginary	$k_{-\beta}$ or k_{-x}	isreal()	Same
Test 1	E_{cat} at pH 4	max(di/dE)	0.72 to 0.77	Same
Test 2	E_{cat} at pH 6	max(di/dE)	0.65 to 0.70	Same
Test 3	CV activation at pH 4 based on change in low-potential vertex from scan 1 to scan 2	$\frac{i(\text{vertex, scan 1})}{i(\text{vertex, scan 2})}$	0.73 to 0.89	0.80 to 0.90 expt = ~85%
Test 4	CA inactivation after 100 s hold at open circuit, as measured experimentally (5 s post hold), pH 4 (like Figure 2B)	$1-\frac{i(\text{5 s post hold})}{i(\text{SS})}$	–0.01 to 0.23	0.02 to 0.12
Test 5	Rate to steady-state after 500 s hold at open circuit, based on currents 5 s post hold, 50 s post hold, and steady-state current, at pH 6	$\frac{i(\text{50 s post hold})-i(\text{SS})}{i(\text{5 s post hold})-i(\text{SS})}$	–0.16 to 2.32	0.12 to 0.60†
Test 6	"X-signature", based on ratio of 20 s post hold and SS current, pH 6 (like Fig. 4B in paper)	$1-\frac{i(\text{20 s post hold})}{i(\text{SS})}$	–0.30 to –0.044	–0.28 to –0.12 expt: –0.20 ± 0.04
Test 7	Identical to test 5, but at pH 4	$\frac{i(\text{50 s post hold})-i(\text{SS})}{i(\text{5 s post hold})-i(\text{SS})}$	–0.36 to 0.91	0.082 to 0.54§
Test 8	CA inactivation after 500 s hold at open circuit, as measured experimentally (5 s post hold), pH 4 (like Figure 2B)	$1-\frac{i(\text{5 s post hold})}{i(\text{SS})}$	0.05 to 0.51	0.25 to 0.45 expt: 0.30 to 0.41

* Determined by iterating between measured and fixed "inactive fraction" (in the sense of Fig. 2B after infinite hold time) at pH 4.0 (55%) and the measured and fixed fraction at pH 5.5 (0%). Maximum iterations was 100; test 9 fails above that. Generation of only negative values fails test 10.
† Experimentally, ~60s are required for two half-lives. The values here set a range of time constants equal to twice that value and half that value.
§ Experimentally, ~75s are required for three half-lives. The values here set a range of time constants equal to twice that value and half that value.

Section S14 Description of Matlab routines

Archives

- There are three ZIP archives of the Matlab routines used for the electrochemical simulation and parameter searches discussed in this manuscript.
- The naming convention is `BMCO_kinetic_scheme`.
- The *`kinetic_scheme`* names correspond directly to those used in Section S3: `P_deadend` (Figure S4), `P_bridge` (Figure S5), `A_deadend` (Figure S6).
- A sample `MConstants.mat` simulation parameter input file is included as a starting point with values that correspond to those used to generate the figures in the paper and the Electronic Supplementary Information

Matlab routines

- There are eight routines in each archive. The *`kinetic_scheme`* names are as above.
- All the routines include a description of the input requirements, display and output settings, and the variables used and their meanings for each kinetic scheme. Undefined variables are set to default values in the code.
- `BMCO_CA_`*`kinetic_scheme_qualifier`*`.m`
  - Simulates chronoamperometry traces and returns a set of vectors with time, catalytic current and fractions of each enzyme state.
  - All CAs have an implicit assumption that substrate diffusion is never limiting (i.e., a sufficiently high electrode rotation rate is used).
  - Qualifier `fully_reduced`: starts CA simulation with 100% of enzyme in Reduced state.
  - If `ShowFigure` is 1 (True), generates three-panel plot on screen with simulated current, simulated potential and fraction of each enzyme state.
- `BMCO_CV_`*`kinetic_scheme`*`.m`
  - Simulates cyclic voltammetry traces and returns a set of vectors with potential, catalytic current, first derivative of the catalytic current and fractions of each enzyme state.
  - All CVs have an implicit assumption that substrate diffusion is never limiting (i.e., a sufficiently high electrode rotation rate is used).
  - If `ShowFigure` is 1 (True), generates plots with CV traces and first derivatives on screen.
- `BMCO_KMO2_`*`kinetic_scheme`*`.m`
  - Simulates the pH and potential dependence of the Michaelis constant (K_M) and the maximum activity (v_{max}), as shown in Fig. 9.
  - Effect of varied O_2 concentration is calculated by multiplying the activity of O_2 (approximately $p_{O2}/p°$) by k_δ.
  - All measurements have an implicit assumption that substrate diffusion is never limiting (i.e., a sufficiently high electrode rotation rate is used).
- `BMCO_pH_profile_`*`kinetic_scheme`*`.m`
  - Simulates the catalytic activity of the enzyme as a function of pH and the apparent fraction of X State by running a series of cyclic voltammetry and chronoamperometry simulations over a range of pH values.
  - If `ShowFigure` is 1 (True), generates plots like those in Figs. 4B & 5 in the main text.
- `BMCO_search_`*`kinetic_scheme`*`.m`
  - Systematic grid search of four variable rate constants for matches to experimental data, as described in Section S13. The spacing between grid points is geometric (i.e., evenly spaced on a logarithmic scale). By default, it applies the test criteria listed under "Narrow tolerance range" in Table S4.
  - Outputs status to screen every 1000 trials. Outputs to the screen hits and fails and current constants every 10000 trials.

    - Creates a log file stored as comma-separated values with timestamps, and values for variables and test parameters for all hits. Log file also contains summary of results. Log file name is composed of search routine name and timestamp.
    - Saves a folder which includes current list of constants and any figures as Matlab figure (.fig) and portable network graphic (.png) files if `SaveFigure` is set to 1 (True). Folder name and contents are timestamped.
- `BMCO_SS_`*`kinetic_scheme`*`.m`
    - Returns the steady-state enzyme concentrations (and catalytic current, if not at open circuit) for a given kinetic scheme and applied electrochemical potential. The equations used in the subroutines were calculated as described at the end of Section S10.
- `BMCO_time_inactive_`*`kinetic_scheme`*`.m`
    - Simulates the apparent inactive fraction of enzyme by running a series of chronoamperometry measurements for a range of pH values and open-circuit hold times.
    - If `ShowFigure` is 1 (True), generates a plot like that in Fig. 2B in the main text.

Section S15 Summary of all searches to match proposed models to experimental data

Section S15.1 Numerical summary of tests

Legend

search	range of values applied when applying test criteria to simulated voltammetry (cf. Section S13)
pK_a(x)	pH value at which the rate of consumption of the X State is equal to its midpoint value (cf. Section S5)
range	number of orders of magnitude between center value for each variable and its minimum or maximum (i.e., $k^{min} = k^{center} \times 10^{-range}$ and $k^{max} = k^{center} \times 10^{+range}$)
grid	number of samples per order of magnitude, spaced evenly on a $\log_{10}$ scale (i.e., $k^{n+1} = k^{n} \times 10^{(1/grid)}$)
tests	total number of variable combinations tested (= (2 range grid + 1)^4)
time per 1000 tests	average clock time for one thousand sets of variables to be tested on a single core of an Intel Core2 Quad Q9400 CPU running at 2.66 GHz with 4 GB RAM running Matlab 7.10.0 (R2010a)
hits	number of sets of variables passing all 11 tests
failing test *n*	number of sets of variables failing test *n* (cf. Table S4)

Table S5(a). "P deadend" searches (cf. Figure S5 and Section S15.3.1)

search	range	grid	tests	time per 1000 tests	hits	failing test 1	failing test 2	failing test 3	failing test 4	failing test 5	failing test 6	failing test 7	failing test 8	failing test 9	failing test 10	failing test 11
wide	2	5	194481	21m21s	1941	126670	453	32716	2262	1003	1837	239	102	27258	0	0
tight	2	5	194481	21m06s	18	126670	453	33429	5175	1116	290	48	24	27258	0	0
refine	0.3	20	390625	32m55s	4806	105280	0	206672	40885	15122	10873	92	6895	0	0	0

Table S5(b). "P bridge" searches (cf. Figure S6 and Section S15.3.2)

search	range	grid	tests	time per 1000 tests	hits	failing test 1	failing test 2	failing test 3	failing test 4	failing test 5	failing test 6	failing test 7	failing test 8	failing test 9	failing test 10	failing test 11
wide	2	5	194481	15m26s	1034	111960	276	22081	1028	654	1218	223	98	22566	73	33270
tight	2	5	194481	15m23s	12	111960	276	22495	2689	817	257	42	24	22566	73	33270
refine	0.3	20	390625	26m33s	4711	105786	0	207608	38991	15340	11051	76	7062	0	0	0

Table S5(c). "A deadend" searches (cf. Figure S7 and Section S15.3.3)

search	range	grid	tests[a]	time per 1000 tests	hits	failing test 1	failing test 2	failing test 3	failing test 4	failing test 5	failing test 6	failing test 7	failing test 8	failing test 9	failing test 10	failing test 11
wide	3	5	1048576	23m19s	0	912399	21	127042	1710	5107	2297	0	0	0	0	0

[a] These tests were run as 16 equally sized partitions of the four-dimensional variable space and included some overlapping search parameters at the boundaries of the search space.

Section S15.2 Range of rate constants that match experimental data

Table S6. Rate constants, their ranges of values that meet the selection criteria, and the values used for the comparison. Variables not tabulated are identical in all simulations and are listed in Table 1 in the main text. Values for $k_{-\beta}$ and k_{+x} are derived from the other four variables. Values for the "P deadend" and "P bridge" schemes are identical.

variable	$k_{\alpha}^{\text{max,low pH}}$	$k_{+\beta}^{\text{low pH}}$	$k_{-\beta}$	k_{γ}^{max}	k_{+x}	$k_{-x}^{\text{low pH}}$
value used	1.6×10^{3}	1.4×10^{-3}	6.6×10^{-4}	5.2×10^{-2}	5.6×10^{-2}	5.9×10^{-1}
geometric mean	6.7×10^{2}	1.6×10^{-3}	7.0×10^{-4}	3.8×10^{-2}	1.1×10^{-1}	6.2×10^{-1}
minimum	2.2×10^{2}	1.1×10^{-3}	3.5×10^{-4}	2.3×10^{-2}	3.0×10^{-2}	4.2×10^{-1}
maximum	1.8×10^{3}	2.7×10^{-3}	1.2×10^{-3}	5.2×10^{-2}	6.4×10^{-1}	1.0×10^{0}
max/min	7.9	2.5	3.5	2.2	21.1	2.5

Section S15.3 Graphical summary of all searches to match proposed models to experimental data and successful matches

Section S15.3.1 "P deadend": X State located at a deadend from Peroxy Intermediate

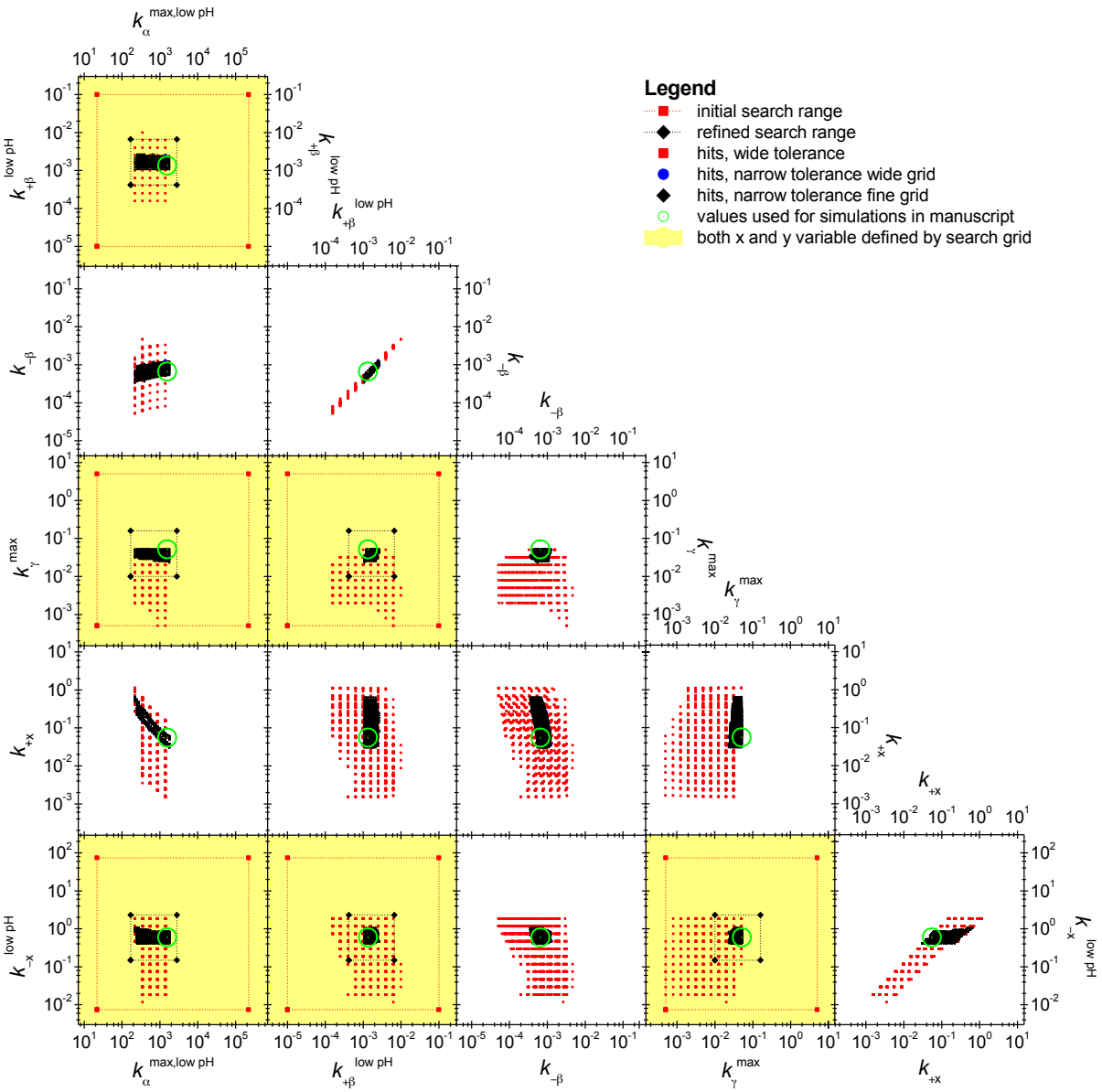

Figure S18. Graphical summary of simulation results for "P deadend" scheme, showing the cross correlation between simulation variables.

Table S7. Center values used for final refinement of variables (cf. Figure S18)

$k_{\alpha}^{max,low\ pH}$	$k_{+\beta}^{low\ pH}$	$k_{-\beta}$	k_{γ}^{max}	k_{+x}	$k_{-x}^{low\ pH}$
7.0×10^{2}	1.7×10^{-3}	7.5×10^{-4}	4.1×10^{-2}	9.3×10^{-2}	5.9×10^{-1}

Section S15.3.2 "P bridge": X State bridges from Peroxy Intermediate to Active Oxidized form

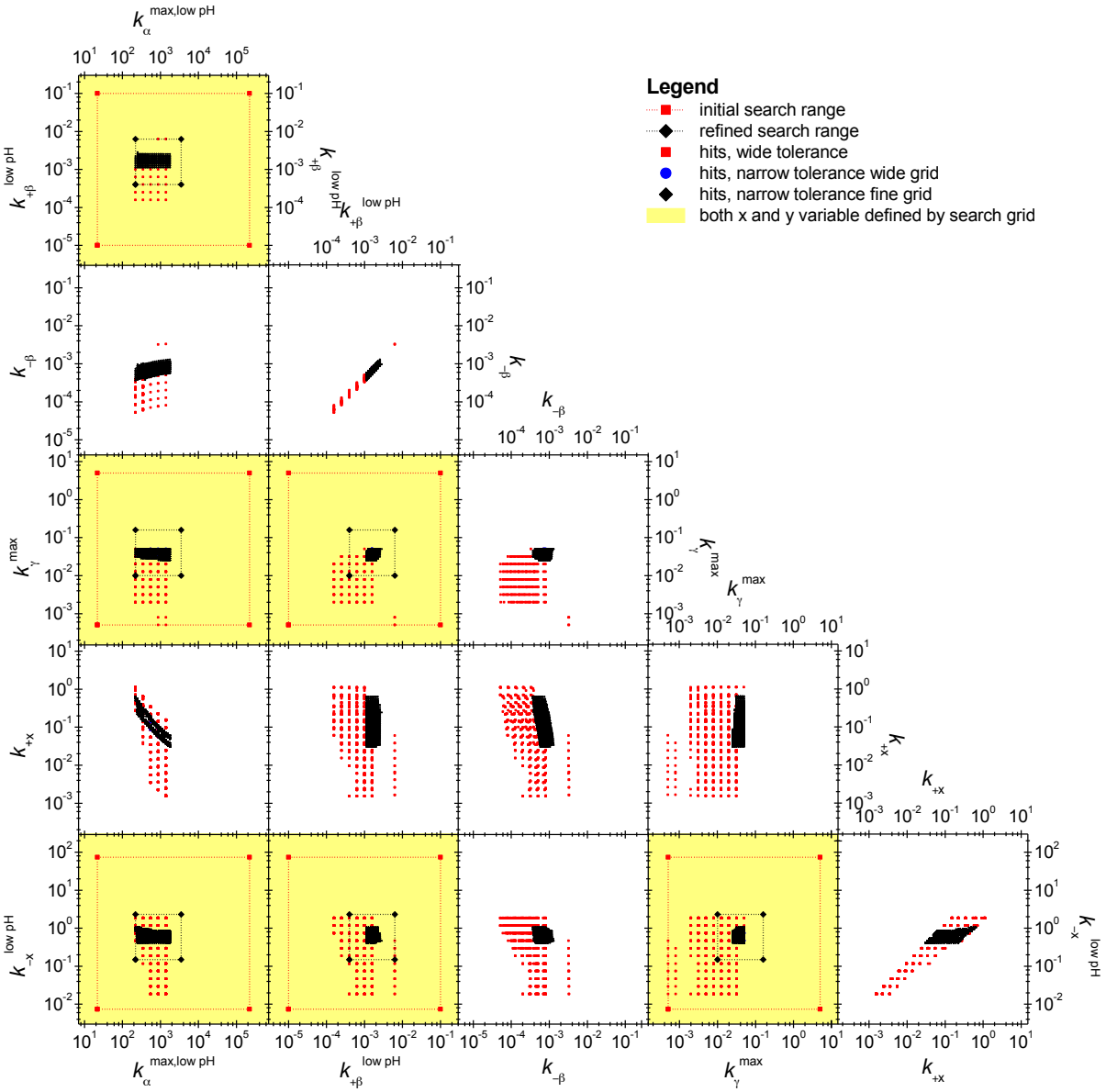

Figure S19. Graphical summary of simulation results for "P bridge" scheme, showing the cross correlation between simulation variables.

Table S8. Center values used for final refinement of variables (cf. Figure S19)

$k_{\alpha}^{\text{max,low pH}}$	$k_{+\beta}^{\text{low pH}}$	$k_{-\beta}$	k_{γ}^{max}	k_{+x}	$k_{-x}^{\text{low pH}}$
8.8×10^{2}	1.6×10^{-3}	7.5×10^{-4}	4.0×10^{-2}	7.2×10^{-2}	5.9×10^{-1}

Section S15.3.3 Graphical summary of hits and misses for "P deadend", "P bridge" and "A deadend"

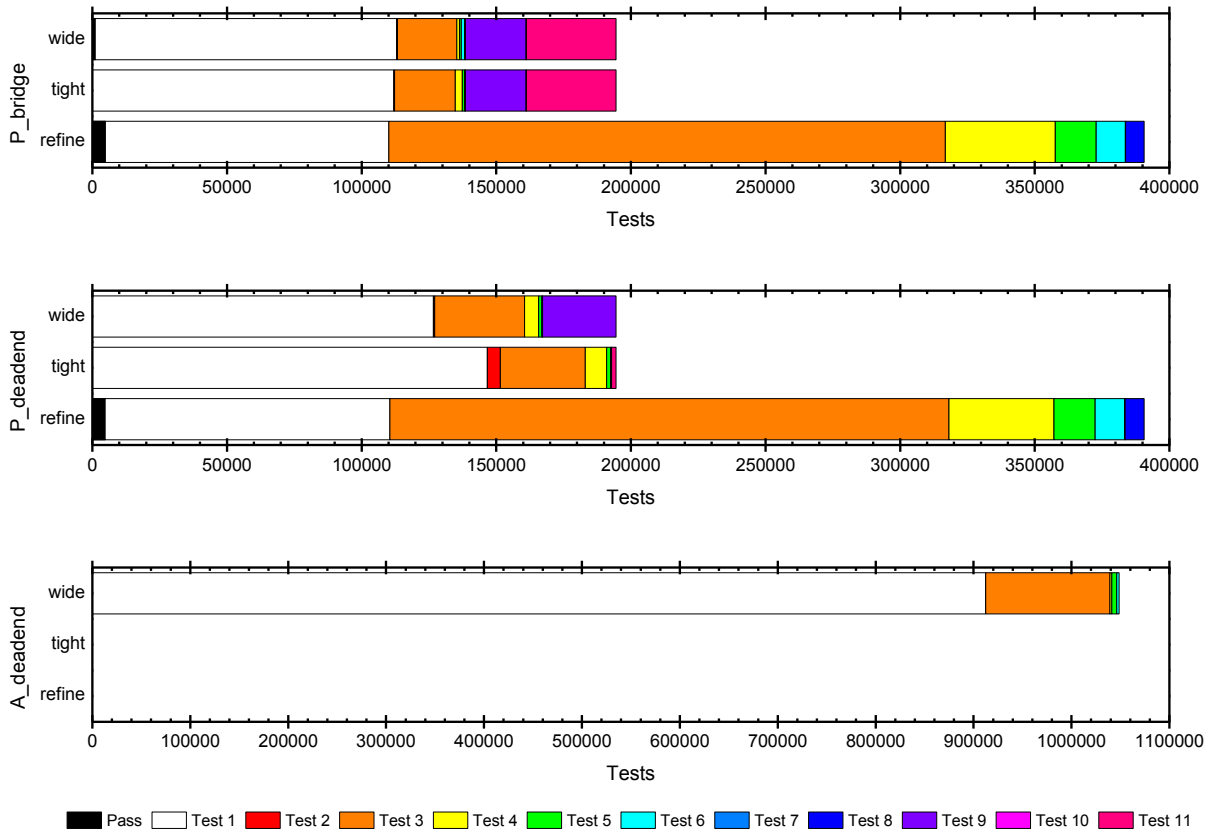

Figure S20. Graphical summary of the data tabulated in Section S15.